Strål
säkerhets
myndigheten
Swedish Radiation Safety Authority

Research

Calibration of models for cladding tube high-temperature creep and rupture in the FRAPTRAN-QT-1.5 program

2021:04

Authors: Lars Olof Jernkvist and Ali R. Massih
Quantum Technologies AB Uppsala Science Park
Report number: 2021:04
ISSN: 2000-0456
Available at: www.ssm.se

SSM perspective

Background

The Swedish Radiation Safety Authority (SSM) follows the research on fuel performance closely. One aspect that is currently being studied in several research projects is the risk of release of fragmented fuel into the primary coolant in case of an accident. This risk depends on complex conditions where one is the possibility and size of a rupture of the fuel rod cladding tube.

This present report describes improvements to the FRAPTRAN-1.5 version extended by Quantum Technologies AB, regarding models for high-temperature cladding creep and rupture. The project is one part of a larger endeavour to update the computer codes that SSM disposes of through Quantum Technologies AB. It was deemed important to do a calibration of the aforementioned models since a previous project showed a need to scale the cladding high temperature creep rate significantly.

Results

In this project, selected model parameters have been calibrated against open literature data. The results shows that it is possible to get results that better reproduce the measured cladding burst times, temperatures, stresses and strains for the considered tests.

The report also discusses the impact of corrosion on cladding high temperature deformation and rupture. It summarizes the mechanisms through which oxygen and hydrogen affect the creep and rupture behaviour, and indicates issues that need further investigation.

Relevance

With this project, SSM has gained a computer code with an improved capability to predict cladding high-temperature rupture behaviour. SSM has also gained insight into the calibration of a model. This is of great importance when reviewing safety analyses for nuclear fuel, especially for assessing assumptions and motives for uncertainties. Furthermore, this project is part of the international development work and enables active participation in international contexts.

Need for further research

The continued development of models for analysing high-temperature creep and rupture behaviour in nuclear fuel is necessary. After this project, it is clear that there is a need for validation against tests of modern cladding materials and for continued development of the effects of corrosion and hydrogen in the cladding. On a longer time scale much research and development remains to fully understand the behaviour of high burnup fuel.

Project information

Contact person SSM: Anna Alvestav
Reference: SSM2018-4296 / 7030270-00

Strål
säkerhets
myndigheten
Swedish Radiation Safety Authority

Authors: Lars Olof Jernkvist and Ali R. Massih
Quantum Technologies AB Uppsala Science Park

2021:04

Calibration of models for cladding tube high-temperature creep and rupture in the FRAPTRAN-QT-1.5 program

Date: February 2021
Report number: 2021:04 **ISSN:** 2000-0456
Available at www.stralsakerhetsmyndigheten.se

This report concerns a study which has been conducted for the Swedish Radiation Safety Authority, SSM. The conclusions and viewpoints presented in the report are those of the author/authors and do not necessarily coincide with those of the SSM.

Calibration of models for cladding tube high-temperature creep and rupture in the FRAPTRAN-QT-1.5 program

Lars Olof Jernkvist and Ali R. Massih

July 17, 2020

Quantum Technologies AB
Uppsala Science Park
SE-751 83 Uppsala, Sweden

Calibration of models for cladding tube high-temperature creep and rupture in the FRAPTRAN-QT-1.5 program

Lars Olof Jernkvist and Ali R. Massih

Quantum Technologies AB
Uppsala Science Park
SE-751 83 Uppsala, Sweden

Quantum Technologies Report: TR20-003V1
Project: SSM 2018-4296

Contents

Summary

This report presents an integral calibration of models for high-temperature behaviour of Zircaloy cladding tubes. The models are intended for analyses of the thermal-mechanical behaviour of light water reactor nuclear fuel rods under conditions expected for loss-of-coolant accidents (LOCAs) in these reactors, and they have been implemented in an extended version of the FRAPTRAN-1.5 computer program. The models are phenomenologically based and strongly interconnected. They deal with cladding tube high-temperature (>1000 K) oxidation, deformation, solid-to-solid phase transformation and rupture.

Selected parameters in these models are calibrated against an open literature database with 150-odd burst tests, carried out on individual test rods with Zircaloy-4 cladding over a wide range of simulated LOCA conditions. The calibration, which is done by use of a Nelder-Mead optimization algorithm, significantly improves the capacity of the models to reproduce the measured cladding burst times, temperatures, stresses and strains for the considered tests. In particular, systematic errors (bias) in the calculated results are practically eliminated by the calibration. Statistical measures for the uncertainty in calculated burst times, temperatures, stresses and strains are evaluated and presented. This information is valuable for assessing uncertainties in future LOCA safety analyses with the calibrated models.

Comparisons of the calibrated models against data from high-temperature burst tests on fuel rods with Zircaloy-2 and ZIRLO cladding show that the models are applicable also to these materials. The calibrated models exhibit a slight tendency to overestimate cladding burst times and temperatures for tests on pre-irradiated fuel rods. Possible effects of pre-irradiation, in particular those related to cladding in-service corrosion and hydrogen pick-up, are discussed in light of experimental data, and suggestions for further model development on these effects are given.

Sammanfattning

Föreliggande rapport presenterar en helhetskalibrering av modeller för simulering av beteendet hos kapslingsrör av Zircaloy vid hög temperatur. Modellerna är avsedda för att analysera det termomekaniska beteendet hos kärnbränslestavar till lättvattenreaktorer vid förhållanden som kan förväntas under haverifall med kylmedelsförlust (LOCA) i dessa reaktorer, och de har implementerats i en utvidgad version av beräkningsprogrammet `FRAPTRAN-1.5`. Modellerna är fenomenologiska och starkt sammankopplade. De hanterar oxidation, deformation, kristallin fastransformation och brott hos kapslingsrören vid hög temperatur (>1000 K).

Utvalda parametrar i dessa modeller kalibreras mot en öppen databas med drygt 150 sprängprov, vilka genomförts på enskilda provstavar av Zirclaoy-4 över ett brett spektrum av simulerade LOCA-förhållanden. Kalibreringen, vilken genomförs med en Nelder-Mead optimeringsalgoritm, förbättrar avsevärt modellernas förmåga att reproducera uppmätta brottidpunkter, brottemperaturer, spänningar och töjningar i de beaktade proven. I synnerhet gäller detta för de systematiska felen (bias), vilka praktiskt taget elimineras av kalibreringen. Statistiska mätetal för osäkerheten i beräknade brottidpunkter, brottemperaturer, spänningar och töjningar beräknas och presenteras. Denna information är värdefull för att uppskatta osäkerheter i framtida LOCA säkerhetsanalyser med de kalibrerade modellerna.

Jämförelser av de kalibrerade modellerna mot data från sprängprov vid hög temperatur av bränslestavar med kapslingrör av Zircaloy-2 och ZIRLO visar att modellerna kan användas även för dessa material. De kalibrerade modellerna uppvisar en svag tendens till att överskatta tid och temperatur vid kapslingsbrott för de prov som genomförts på förbestrålade bränslestavar. Tänkbara effekter av förbestrålning, i synnerhet de som kan relateras till kapslingskorrosion och väteupptag under bränslestavens livstid, diskuteras mot bakgrund av tillgängliga data och förslag ges till fortsatt modellutveckling avseende dessa effekter.

1 Introduction

Computational analyses of the behaviour of nuclear fuel rods under postulated loss-of-coolant accident (LOCA) conditions are essential in safety evaluations of light water reactors (LWRs). The exceptional conditions and the complex interactions of physical phenomena under LOCA call for specific computational models, much different from those used for analysing fuel rod behaviour under normal reactor operation [1]. More precisely, under LOCA, the fuel rods experience an excursion to high temperature concurrently with high internal overpressure as the primary coolant water is lost. This condition can cause excessive outward expansion (ballooning) of the zirconium-based cladding tube by high-temperature viscoplastic (creep) deformation. The high-temperature deformation is affected by metal-steam reactions (oxidation) and a crystallographic phase transition from hexagonal (α-phase) to cubic (β-phase) crystal structure in the zirconium alloy at temperatures above 1000-1100 K: the transition temperature depends on the cladding alloy composition, the heating rate and the amount of oxygen and hydrogen picked up by the cladding metal. As a combined result of excessive deformation and oxidation, the cladding tube may rupture before the emergency core coolant system brings the fuel rod temperature back to normal within a few minutes, and there is also a risk that the cladding breaks by stresses induced by thermal shock when the fuel rod is re-wetted [2].

Separate but strongly interconnected sub-models for the aforementioned phenomena, i.e high-temperature creep, metal-steam reactions, phase transformation and rupture, pertinent to zirconium alloy cladding tubes under LWR LOCA conditions, were formulated in earlier research projects for the Swedish Radiation Safety Authority (SSM) [3] and implemented in an extended version of the `FRAPTRAN-1.5` fuel rod analysis program [4], henceforth referred to as `FRAPTRAN-QT-1.5` [5]. The phase transformation model was developed in-house by Quantum Technologies [6], while models for other phenomena were taken from open literature sources with no or moderate modification. In fact, several alternative models for each phenomenon are implemented in `FRAPTRAN-QT-1.5`, and they can be used in any combination at the analyst's choice [5].

Over the years, `FRAPTRAN-QT-1.5` and the aforementioned set of models have been used for evaluating various LOCA-simulation tests and experiments. Both separate effect tests on the cladding high-temperature behaviour [7] and integral-type LOCA-simulation experiments [3, 8–11] have been evaluated over a fairly long period of time, in parallel with model improvements. The experience gained from this work can be summarized in two general conclusions: Firstly, cladding high-temperature oxidation, deformation and solid-to-solid phase transformation are strongly interconnected phenomena. Models for these phenomena must for this reason be harmonized and *collectively* calibrated against experimental data to achieve best possible accuracy for all calculated properties of interest. When models are taken from various sources and combined without harmonization and integral calibration, the calculated results usually exhibit systematic errors (bias). Secondly, the models may also need adaptation to the fuel rod analysis computer program in which they are used. The reason is that the phenomenological models take input in the form of local temperature and stress state from the host program and return local cladding strains and other calculated properties to the program. Temperatures, stresses and strains are calculated and treated differently from one computer program to another, e.g. with regard to the radial-axial-circumferential variation of these properties in the cladding material and/or the

kinematic description of large deformations and strains [12]. A computational model, designed for a specific host program, may therefore need to be modified and/or re-calibrated, when used in another program.

In answer to these findings, this report presents an integral calibration of models for high-temperature behaviour of Zircaloy cladding that are available in the current version of FRAPTRAN-QT-1.5 [5]. The objective is twofold: to reduce the bias observed for the creep and burst models in our previous evaluations of LOCA-simulation tests, and to introduce and calibrate improved models for cladding phase transformation and metal-steam reactions in FRAPTRAN-QT-1.5. The latter models are new, and have not been used in earlier evaluations of LOCA tests and experiments.

The calibration is done against a primary database with results from 151 single-rod burst tests, carried out under simulated LOCA conditions on un-irradiated and pre-irradiated fuel rods with Zircaloy-4 cladding. Selected parameters in the models for cladding high-temperature creep and burst are first calibrated against this database by use of a Nelder-Mead optimization algorithm, such that the relative differences between calculated and measured values for burst time and burst hoop stress are minimized. Next, the optimized models are assessed against data from high-temperature burst tests on fuel rods with Zircaloy-2 and ZIRLO cladding, with the aim to test and verify the applicability of the models to these materials.

The report is organized as follows:

Section 2 summarizes the experimental data used for model calibration, describes the models used for Zircaloy cladding high-temperature behaviour in FRAPTRAN-QT-1.5, defines the model parameters selected for optimization, and presents the applied optimization procedure.

The results of the model calibration are presented and discussed in Section 3. The optimized model parameters are presented. Experimental data are compared with results calculated with both the original and the calibrated models, in order to assess the improvements made. The calibrated models are also compared with high-temperature burst test data for Zircaloy-2 and ZIRLO cladding. Possible effects of long-term in-reactor operation on the fuel behaviour during LOCA are also discussed, in particular the effects of cladding corrosion and hydrogen pick-up on cladding high-temperature ballooning and burst.

Finally, Section 4 summarizes the work and the most important conclusions that can be drawn from it. Moreover, suggestions are also given for further model development.

2 Calibration method

Selected parameters in models for Zircaloy cladding high-temperature creep and rupture were calibrated against results from 151 cladding burst tests, conducted in six experimental series. In summary, each test in the database was simulated with a specific set of model parameters. The calculated results for all tests were then compared with experimental results and a scalar measure of the goodness of fit was determined for this specific set of model parameters. By repeating this process for different sets of model parameters within an optimization algorithm, an optimal fit for the model parameters could be determined. In the following, we describe the experimental database, the computer models and the calibrated parameters, and how an optimal fit of these parameters to the data was found.

2.1 Experimental data used for model calibration

Altogether 151 burst tests on Zircaloy-4 (Zr-1.4Sn-0.2Fe-0.1Cr by wt%) cladding tube samples were used for model calibration in this study. All of the tests were done in steam environment by heating a single internally overpressurized tube sample at a time until the sample ruptured. The most important experimental parameters were the sample internal overpressure and heating rate. The results from each test comprise time to cladding burst (rupture), burst temperature and hoop creep strain at burst. The tests included in the database were selected based on availability of information: for each test included in the database, sufficient information is available in open literature sources to allow simulations of the test, and key test results are reported. Hence, the considered tests allow one-to-one comparisons of calculated versus measured burst time, burst temperature and burst hoop strain.

The tests selected for model calibration were conducted in six different experimental series. Key parameters for these test series are summarized in Table 1. Except for the KfK-83(F) and KfK-83(I) series, the tests were done out-of-reactor on fresh (un-irradiated) cladding samples. The KfK-83 tests were done in the FR2 research reactor, Germany, using both fresh (F) and pre-irradiated (I) test rods. The pre-irradiated test rods had UO_2 fuel burnups ranging from 2.5 to 35 MWd(kgU)$^{-1}$. In most of the out-of-reactor tests, the cladding tubes were heated by internal electrical resistance heaters. In the KfK-88 test series, the internal heating was supplemented by external heating from the shroud enclosing the sample, resulting in exceptionally uniform temperature within the samples. In the BARC-17 tests, direct electrical (Joule) heating was used. It seems that this kind of heating resulted in large temperature gradients in the samples, both in the axial and circumferential direction [13].

Most of the data in the considered database were assessed and found useful for model calibration in an earlier project [7]. More precisely, the selected tests were found to be fairly well documented and the cladding materials and testing methods are well described. Sufficient data are given to allow simulations of individual tests. The BARC-17 dataset [13] is recent, and consequently, it was not included in our 2015 assessment [7]. The BARC-17 tests were conducted on Zircaloy-4 cladding to Indian pressurized heavy water reactor (PHWR) fuel rods. The geometry of this cladding is different from that of typical LWR fuel cladding, which is the design studied in the other test series.

Table 1: Zircaloy-4 cladding burst test data used for model calibration. All test series except for BARC-17 are summarized in [7]. A complete description of the data used for model calibration is given in Appendix A.

Test series	# tests	Test type	Heating type	D_o [mm]	W_o [mm]	ΔP [MPa]	$\dot{T}$ [Ks^{-1}]	T_b [K]	ε_b [%]	Literature source
ORNL-79	40	OR	Internal	10.920	0.635	0.8 - 20.8	4.8 - 30.6	961 - 1444	13.1 - 58.2	[14–16]
KfK-83(F)	19	IR	Int(nucl)	10.750	0.725	2.1 - 11.6	6.1 - 24.7	1020 - 1288	23.1 - 49.5	[17, 18]
KfK-83(I)	22	IR	Int(nucl)	10.750	0.725	2.4 - 12.5	7.3 - 16.7	981 - 1218	23.9 - 51.3	[17, 18]
KfK-88(C)	23	OR	Int+Ext	11.900	0.550	0.6 - 9.8	1.1	976 - 1285	21.5 - 72.8	[19, 20]
KfK-88(N)	18	OR	Int+Ext	11.900	0.550	2.7 - 9.4	1.1	980 - 1162	47.0 - 65.8	[19, 20]
BARC-17	29	OR	Direct	15.200	0.400	0.3 - 7.4	5.0 - 19.0	871 - 1372	8.5 - 51.7	[13]
Total:	151	–	–	10.75 - 15.20	0.400 - 0.725	0.3 - 20.8	1.1 - 30.6	871 - 1444	8.5 - 72.8	

OR/IR: Out-of-reactor/In-reactor test; D_o/W_o: Cladding as-fabricated outer diameter/wall thickness; $\Delta P, \dot{T}$: Sample internal overpressure and heating rate in test; T_b/ε_b: Measured burst temperature and hoop logarithmic burst strain.

Our previous assessment of the data [7] contains the test results in a format taken directly from the literature sources. This makes it difficult to compare the data from one test series to another, since pressures, heating rates, stresses and strains are defined somewhat differently from one literature source to another. For this reason, the data are presented in a consistent format in Appendix A, where we also define the Cauchy hoop stress and the logarithmic (true) hoop strain. These measures of stress and strain are consistently used throughout the report.

Figure 1 shows the measured Cauchy hoop stress at time of cladding burst plotted versus measured burst temperature for all tests. The general trend of the data is clear: the higher the temperature, the lower the burst stress. The scatter is partly due to differences in heating rate and rod internal overpressure among the tests, but also to the inevitable scatter in hoop burst strain: as explained in Appendix A, the Cauchy burst stress depends exponentially on the burst strain. The measured hoop logarithmic strain at time of burst is plotted versus measured burst temperature in Figure 2. It is difficult to discern any clear tendency in the burst strain data as a whole, although some trends can possibly be identified for individual test series.

We also note that the burst strains observed in the KfK-88 test series for temperatures below 1150 K are generally higher than burst strains in other tests. This is probably a result of the uniform and slow heating used in the KfK-88 tests; compare Table 1. In fact, the scatter observed in burst strain data from cladding burst tests is attributed primarily to circumferential (azimuthal) temperature gradients that arise in the samples during testing [19, 21]. Also very moderate temperature differences along the cladding circumference lead to localization of the creep deformation, bending of the sample and to cladding failure at a lower overall hoop strain than if the sample temperature had been perfectly uniform. A perfectly uniform temperature cannot be achieved in practice, but some heating methods are better than others to produce near-uniform temperature distributions. Consequently, both the scatter in burst strain data and the average burst strain level depend on the heating method used in the testing.

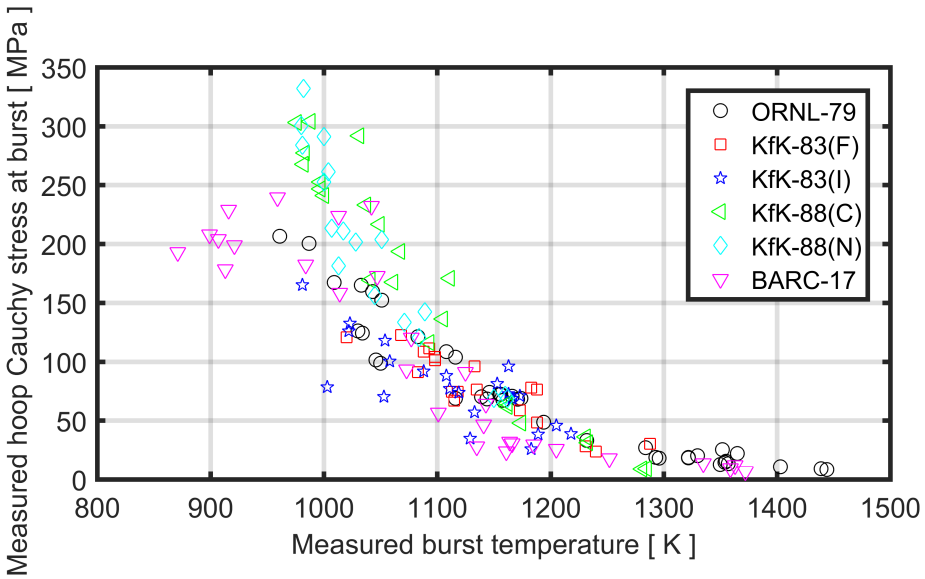

Figure 1: Measured Cauchy hoop stress versus temperature at time of cladding burst. The legend refers to the six test series summarized in Table 1.

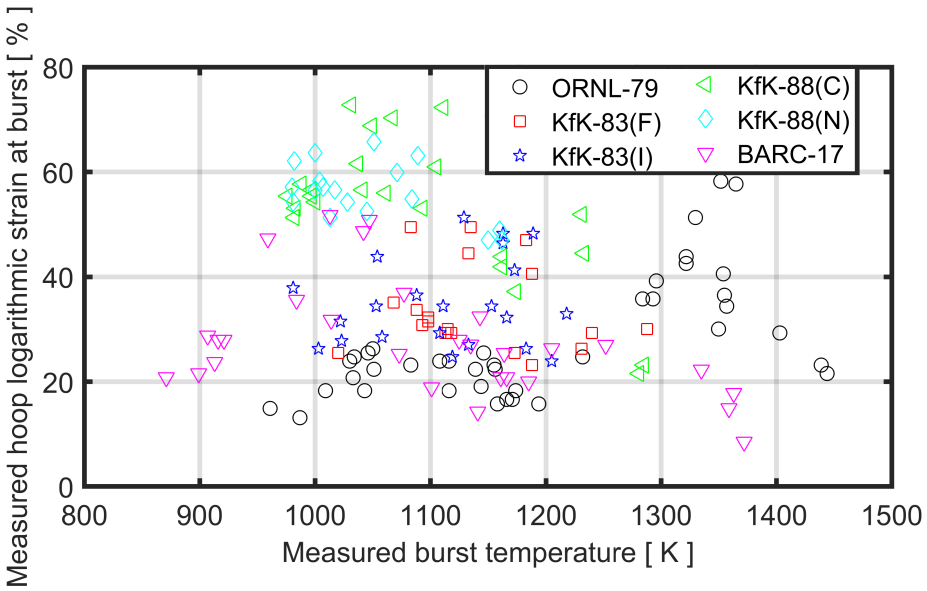

Figure 2: Measured hoop logarithmic strain versus temperature at time of cladding burst.

2.2 Computer models and calibrated model parameters

The computational models for cladding high-temperature behaviour in `FRAPTRAN-QT-1.5` are phenomenological and address the phenomena described in Section 1. More precisely, separate but closely interlinked submodels are used for high-temperature zirconium alloy cladding-steam reactions, phase transformation (solid-to-solid $\alpha \Leftrightarrow \beta$), high-temperature creep deformation, and eventually, rupture. The main quantities calculated by the models are (1) oxygen parameters, generically denoted by x_i, which can be either the total amount of oxygen picked up by the cladding during the oxidation process, the thickness of the inner/outer surface oxide layer, or the excess oxygen concentration in the cladding metal layer; (2) the volume fractions of β-Zr, y; (3) the cladding effective strain due to creep, ε_e; (4) and the cladding burst (hoop) stress, σ_b. All these quantities are coupled through a set of kinetic equations and a burst criterion. For a specific point in the cladding material, they may be expressed generically in the form

$$\frac{\mathrm{d}x_i}{\mathrm{d}t} = f_1(x_i, T, \varepsilon_e), \tag{1}$$

$$\frac{\mathrm{d}y}{\mathrm{d}t} = f_2(y, x_i, T), \tag{2}$$

$$\frac{\mathrm{d}\varepsilon_e}{\mathrm{d}t} = f_3(T, \sigma_e, y, x_i), \tag{3}$$

$$\text{and} \quad \sigma_b = f_4(x_i, T, y), \tag{4}$$

where f_i, $i = \{1, 2, 3\}$ are the respective functions for the time evolution of the variables during the transient, σ_e is the cladding von Mises effective stress, and $T = T(\mathbf{r}, t)$ is the cladding temperature, which in general, is a function of space $\mathbf{r}$ and time t, controlled by power and/or coolant boundary conditions during the accident. Moreover, f_4 is a purely empirical function of cladding oxygen concentration and temperature or phase composition. The burst criterion can alternatively be defined in terms of burst strain rather than stress. The three interlinked first-order differential equations (1) - (3) are solved numeri-

cally to obtain the time evolution of the respective variables during the transient. They are solved in each integration point of the discretized cladding geometry, based on the local stress and temperature calculated by other modules of the FRAPTRAN-QT-1.5 program. The explicit forms of f_i, $i = \{1, 2, 3, 4\}$ used specifically for Zircaloy cladding in this report are described in the following subsections. A general presentation of all models and options available in FRAPTRAN-QT-1.5 is available in [5].

The cladding high-temperature models described above have been implemented not only in FRAPTRAN-QT-1.5, but also in a stand-alone MATLAB program. This program is called ftmat and uses a thin-shell mechanical model for an internally pressurized cladding tube for calculating the stress state in the material. This eliminates the space dependence and renders the computed parameters only functions of time. More precisely, the stress state in the internally pressurized cladding tube is calculated from thin shell theory (boiler formulas), considering large deformations of the cladding tube. Hence, the normal Cauchy (true) stress components in the (r, θ, z) cylindrical coordinate system aligned with the cladding tube are calculated from

$$\sigma_{rr}(t) = 0, \tag{5}$$

$$\sigma_{\theta\theta}(t) = \Delta P(t) \frac{R_{av}(t)}{W(t)}, \tag{6}$$

$$\sigma_{zz}(t) = \frac{\Delta P(t)}{2} \frac{R_{av}(t)}{W(t)}, \tag{7}$$

where ΔP is the internal overpressure in the cladding tube, R_{av} is the cladding average radius, and W is the cladding thickness (oxide layer included). All these parameters are in ftmat assumed to vary with time, but not with space. From the above relations, it follows that the von Mises effective stress is

$$\sigma_e(t) = \frac{\sqrt{3}\Delta P(t)}{2} \frac{R_{av}(t)}{W(t)}. \tag{8}$$

The effective stress in equation (8) is used for calculating the effective creep rate.

It should be remarked that, in ftmat, cladding deformations are assumed to result from creep only; contributions from thermo-elasticity and time-independent plasticity are neglected. Moreover, the creep deformation is assumed to be isotropic, which means that the Levy-Mises flow rule applies [22]. With the stress state defined by equations (5)-(7), this flow rule gives the components of cladding creep strain rate through

$$\dot{\varepsilon}_{rr} = -\dot{\varepsilon}_e \frac{\sqrt{3}}{2}, \tag{9}$$

$$\dot{\varepsilon}_{\theta\theta} = \dot{\varepsilon}_e \frac{\sqrt{3}}{2}, \tag{10}$$

$$\dot{\varepsilon}_{zz} = 0, \tag{11}$$

where $\dot{\varepsilon}_e$ is the effective creep strain rate, calculated as a function of effective stress, temperature, etc., through correlations, as given by equation (3). The cladding average radius and wall thickness depend on the cladding creep deformation through equations (A.3) and (A.4) in Appendix A.

In the work presented here, `ftmat` was used instead of the full `FRAPTRAN-QT-1.5` computer program for simulating the cladding burst tests. By this, input and output handling could be much simplified, and efficient optimization algorithms that are available in the MATLAB Optimization Toolbox could be used [23]. It was verified that `ftmat` and `FRAPTRAN-QT-1.5` give practically identical results when the same high-temperature cladding material properties models are used. Input to `ftmat` consists of cladding material options, various modeling options, cladding dimensions, initial cladding temperature and its heating rate, overpressure in the cladding and its rate of change, if any. For the purpose of model calibration, the input also comprises a set of tuning factors (multipliers) for selected model parameters; see section 2.3. The `ftmat` program returns as output calculated cladding burst time, cladding burst temperature, cladding burst hoop strain/stress, and the volume fraction of β-phase at burst.

When simulating single-rod burst tests with our computational models, the following simplifying assumptions were made for each sample:

- The heating rate was assumed to be constant throughout the test;
- The internal overpressure was assumed to be constant throughout the test. In most experiments, the internal overpressure increases slightly as the sample is heated, passes through a maximum, and then drops rapidly as the sample internal volume increases as a result of cladding ballooning prior to rupture. The initial pressure, the maximum pressure and the final burst pressure are usually reported from the tests. All calculations in this report were done with the internal pressure equal to the average of the reported initial and maximum pressures;
- The steam supply to the test chamber was assumed sufficient to feed the metal-steam reactions (no steam starvation);
- Axial symmetry was assumed for the cladding geometry and heating conditions, i.e. temperature differences along the cladding circumference were neglected;
- Axial gradients in cladding deformation and temperature were not considered;
- Effects of cladding pre-irradiation on the high-temperature behaviour were considered by accounting for the cladding pre-test hydrogen concentration, in case this concentration was known for the sample. If not, the pre-test hydrogen concentration was assumed to be 10 wppm.

The last point is relevant for the KfK-83(I) test series, for which the hydrogen concentration of the cladding samples is unknown. In fact, virtually no information on irradiation-related pre-test conditions of the cladding used in these tests is available in the open literature [17, 18].

2.2.1 Cladding metal-steam reactions

In `FRAPTRAN-QT-1.5`, empirical correlations are used for calculating the cladding metal-steam reactions at high temperature trough equation (1). The parameters x_i in this equation corresponds to: (i=1) total oxygen uptake; (i=2) excess oxygen in solid solution in the cladding metal; (i=3) oxide layer thickness at the cladding outer surface; (i=4) oxide layer thickness at the cladding inner surface. The last parameter is calculated only after cladding

rupture, when steam is supposed to enter into the pellet-cladding gap through the cladding breach.

Correlations are available for various cladding materials; see [5] for a description of the available options in FRAPTRAN-QT-1.5. In the work presented here, we have used the correlations by Leistikow and Schanz [24]. This is one of four alternative models available for Zircaloy-4 cladding in FRAPTRAN-QT-1.5 [5]. The reason for using this particular model is that it has been identified as the best option for temperatures below 1800 K [25]. It was not used in earlier evaluations of LOCA simulation tests by Quantum Technologies. These evaluations were done with the model by Cathcart and co-workers, which is the default in the standard version of FRAPTRAN-1.5 [4]. Figure 3 presents a comparison of the four alternative models with regard to calculated total oxygen uptake versus time at a constant temperature of 1200 K. The parameters in the Leistikow-Schanz correlations have not been calibrated or modified in the work presented here. As indicated by equations (2)-(4), the correlations used for the cladding metal-steam reactions are important, since these reactions affect the high-temperature deformation and burst behaviour of the cladding.

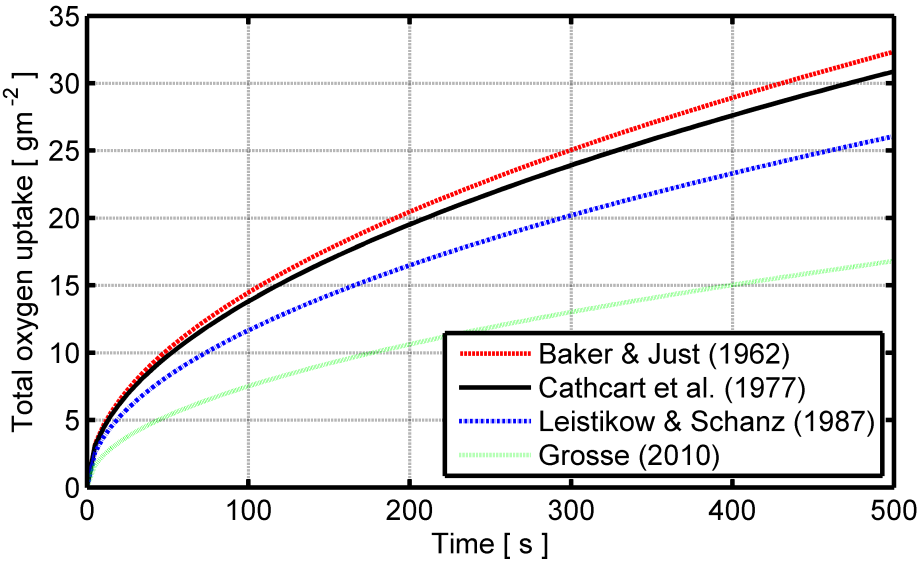

Figure 3: Total oxygen uptake in the cladding versus time at a constant temperature of 1200 K, calculated with the high-temperature metal-steam reaction correlations available for Zircaloy-4 in FRAPTRAN-QT-1.5 [5].

2.2.2 Cladding phase transformation kinetics

The α/β phase composition of the material is essential for calculating creep deformation of zirconium alloy cladding tubes at high temperature. The phase composition depends primarily on temperature, alloy composition and metal excess oxygen concentration, but it is also affected by metal hydrogen content and the heating/cooling rate.

A new model for the phase transformation kinetics of Zircaloy cladding was recently developed and implemented in FRAPTRAN-QT-1.5 [6]. This model was used, without modifications, in the work presented here. In comparison with the earlier model in

FRAPTRAN-QT-1.5, which is still available as an option in the program, the new phase transformation model is applicable to a wider range of heating/cooling rates, and it also considers effects of hydrogen in solid solution within the cladding metal; see Section 3.3.

2.2.3 Cladding creep deformation

Several models for cladding high-temperature creep are available in FRAPTRAN-QT-1.5, by which the effective creep rate can be calculated as a function of temperature, effective stress, phase composition and cladding oxygen content; compare equation (3). Since the creep deformation of Zr-base alloys is very different in α-phase and β-phase, all models have separate creep rate correlations for the two phases. If the two phases coexist, the effective mixed-phase creep rate is calculated by weighting the single-phase creep rates $\dot{\varepsilon}_{e\alpha}$ and $\dot{\varepsilon}_{e\beta}$ with the β-phase volume fraction y (-) through

$$\dot{\varepsilon}_{e\alpha+\beta} = (1-y)\,\dot{\varepsilon}_{e\alpha} + y\,\dot{\varepsilon}_{e\beta}. \tag{12}$$

As an alternative, the interpolation can be done by weighting the creep model parameters with respect to the phase composition, after which the weighted parameters are used for calculating the effective creep strain rate. This procedure is equivalent to calculating the mixed phase effective creep strain rate through logarithmic interpolation, i.e. through

$$\dot{\varepsilon}_{e\alpha+\beta} = \dot{\varepsilon}_{e\alpha}^{(1-y)} \cdot \dot{\varepsilon}_{e\beta}^{\,y}. \tag{13}$$

In FRAPTRAN-QT-1.5, the linear interpolation defined by equation (12) is the default method, but logarithmic interpolation is available as an option [5].

In this work, we apply the Zircaloy-4 high-temperature creep model by Rosinger [26, 27]. According to this model, the steady-state effective creep strain rate in pure α- or β-phase material, $\dot{\varepsilon}_e$ (s^{-1}), is correlated to temperature T (K), von Mises effective stress, σ_e (Pa), and excess oxygen weight fraction in the cladding metal layer, x_{Met} (-), through a Norton-type creep law

$$\dot{\varepsilon}_e = A_c\, e^{-B_c x_{Met}}\, e^{-Q_c/RT} \sigma_e^n. \tag{14}$$

In equation (14), the model parameters A_c, B_c, Q_c and n are constants, which are different for the α- and β-phase; see Table 2. R is the universal gas constant.

Table 2: Constants used in Rosinger's model [26, 27] for calculating high-temperature Zircaloy-4 cladding creep in single-phase domains through equation (14).

Phase domain	A_c ($s^{-1}Pa^{-n}$)	B_c (-)	Q_c/R (K)	n (-)
α	4.000×10^{-32}	342	38487	5.89
β	1.650×10^{-22}	0.0	17079	3.78

Hence, the creep model contains altogether eight constant parameters. Of these parameters, it seems that Q_c and n have firm experimental support, not only by the tests performed by Rosinger himself, but also by other studies [28–32]. The parameter B_c, which defines the strengthening effect of oxygen dissolved in the cladding metal, is underpinned by early experiments on Zircaloy-2 (Zr-1.5Sn-0.2Fe-0.1Cr-0.05Ni by wt%) by Burton et al. [28]

and Choubey et al. [30]. Their results are concordant for α-phase metal, where both studies showed that dissolved oxygen in the metal significantly lowered the creep rate. For β-phase metal, Burton and co-workers reported no effect of oxygen ($B_c = 0$), whereas Choubey and co-workers reported a weak but still noticeable effect ($B_c \approx 130$).

In the present work, the coefficients A_c for α- and β-phase creep were calibrated against the burst test data. Attempts were initially made to also calibrate the parameters B_c for both the α- and β-phase, but this proved unsuccessful. The reason is that the cladding samples that fail under high stress and low temperature already in the α-phase usually have very low excess oxygen concentrations. Likewise, the samples that reach β-phase are in most cases heated so rapidly that they maintain a low oxygen concentration until burst. Consequently, for most samples in the database, the factor $\exp(-B_c x_{Met})$ is close to unity over a wide range of B_c, and this parameter could therefore not be reliably fitted to the considered data.

Finally, we note that the Ashby-Verall type creep model that is available in `FRAPTRAN-QT-1.5` for modelling the contribution of inter-phase interface sliding in the mixed ($\alpha+\beta$)-phase region was not used in the present work [5]. The contribution from this creep mechanism is significant only at very low stress, typically at $\sigma_e < 5$ MPa [33], which is far below the stress level experienced by the cladding samples in the considered database.

2.2.4 Cladding burst criterion

Cladding high-temperature burst (rupture) may in `FRAPTRAN-QT-1.5` be modelled by any of nine different failure criteria that are available as options in the program [5]. The criteria are defined as thresholds for either cladding hoop strain or hoop stress. These thresholds depend primarily on cladding temperature, but they may also account for heating rate and oxygen concentration in the cladding metal. They are empirically based, and most of them are applicable to Zircaloy cladding [5].

In earlier work [3, 7], we identified the best-estimate burst criterion by Rosinger [26] as the best option for Zircaloy cladding, since it was found to reproduce the results of burst tests on Zircaloy and first generation ZIRLO (Zr-1.0Sn-1.0Nb-0.1Fe by wt%) cladding fairly well, when used together with other high-temperature cladding models in `FRAPTRAN-QT-1.5`. However, the criterion exhibited systematic errors with regard to burst time, burst stress and burst strain. To remove this bias, we proposed in [3, 7] to calibrate the burst criterion together with the applied creep model. We also proposed to reformulate the burst criterion, so that it takes the excess oxygen concentration in the cladding metal, rather than the total oxygen uptake, as an input parameter for calculating the burst stress [3, 7]. Here, we make the suggested improvements. We also take the opportunity to slightly modify the original criterion, such that the applied α/β-phase boundary temperatures agree with those used for Zircaloy in our phase transformation model; see section 2.2.2. More precisely, the original criterion defines the threshold hoop Cauchy stress, σ_b (Pa), for cladding high temperature burst as a function of temperature, T (K), and total weight fraction of oxygen picked up by the cladding in high-temperature metal-steam reactions, x_{Tot} (-), through

$$\sigma_b = A_b \, e^{-B_b T} \, e^{-\left(\frac{x_{Tot}}{9.5\times10^{-4}}\right)^2}, \tag{15}$$

where different values for the constant model parameters A_b and B_b are used in the α-, β-

and mixed-phase ($\alpha+\beta$) regions. To the best of our knowledge, the temperature-dependent term in this formulation is based on the early work of Brzoska et al. [34]. The formulation was later adapted and extended by Rosinger [26], who added the oxygen-dependent term. Rosinger proposed two sets of constants for the temperature-dependence [26]: one best-estimate fit to his Zircaloy-4 data and an upper bound model to the same data. Both sets of constants are summarized in Table 3.

Table 3: Constants used for equation (15) by Rosinger [26]. The two sets of constants define Rosinger's upper bound and best estimate burst stress criteria for Zircaloy-4.

	Upper bound		Best estimate	
Temperature region (K)	A_b (Pa)	B_b (K^{-1})	A_b (Pa)	B_b (K^{-1})
873 to 1104	5.04×10^{9}	2.64×10^{-3}	1.00×10^{10}	4.10×10^{-3}
1104 to 1260	7.15×10^{13}	1.13×10^{-2}	3.59×10^{12}	9.43×10^{-3}
1260 to 1873	1.52×10^{9}	2.76×10^{-3}	2.09×10^{8}	1.69×10^{-3}

In this work, three modifications were made to Rosinger's best-estimate burst criterion. Firstly, the total weight fraction of excess oxygen in equation (15) was replaced with the excess oxygen concentration in the cladding metal, x_{Met} (-). Hence, the modified criterion reads

$$\sigma_b = A_b\, e^{-B_b T}\, e^{-\left(\frac{x_{Met}}{C_b}\right)^2}, \tag{16}$$

where C_b is a new constant parameter to be determined from experimental data. In fact, the best-estimate value for C_b will depend on the correlations used for calculating x_{Met}, since *measured* data for x_{Met} (or x_{Tot} for that matter) in burst test samples rarely exist. As in the original formulation of the criterion, we expect C_b to be independent of the material's phase composition. Secondly, the original phase boundary temperatures 1104 and 1260 K were changed to 1075 and 1250 K for consistency with the model applied for phase transformation kinetics [6]. Thirdly, the constant parameters A_b and B_b were re-calibrated against the burst test data presented in section 2.1. Since the burst stress σ_b in equation (16) should be a continuous function with regard to temperature, two constraints are enforced on A_b and B_b at the phase boundary temperatures. Hence, including C_b, there are altogether five parameters for the burst criterion in equation (16) that were fitted to experimental data.

2.3 Parameter optimization method

As described above, two constant parameters for the cladding high-temperature creep model and five constants for the burst criterion were identified as suitable for optimization by fitting to the Zircaloy-4 burst test data in section 2.1. An essential part of any parameter optimization is to define a scalar measure of how well the models reproduce the considered data. This measure is usually referred to as a loss function, or objective- or cost function, since it can be viewed as being a function of the model parameters, **c**, that are to be optimized [35]. Here, the loss function was taken to be the sum of the l^2-norms (Euclidean norms) of the relative differences between calculated and measured burst time, t_b,

and Cauchy hoop stress at time of burst, σ_b, respectively. Mathematically, the applied loss function, $\phi(\mathbf{c})$ (-), can be written

$$\phi(\mathbf{c}) \quad = \quad l^2\big(\mathbf{D}_r(t_b)\big) \quad + \quad l^2\big(\mathbf{D}_r(\sigma_b)\big), \tag{17}$$

where the l^2-norms of the vectors containing relative differences for each of the tests, $\mathbf{D}_r$, are given by

$$l^2\big(\mathbf{D}_r(t_b)\big) \quad = \quad \sqrt{\sum_{i=1}^{n}\left(\frac{t_{bi}^{calc}(\mathbf{c})}{t_{bi}^{meas}}-1\right)^2}, \tag{18}$$

$$l^2\big(\mathbf{D}_r(\sigma_b)\big) \quad = \quad \sqrt{\sum_{i=1}^{n}\left(\frac{\sigma_{bi}^{calc}(\mathbf{c})}{\sigma_{bi}^{meas}}-1\right)^2}. \tag{19}$$

In equation (18), t_{bi}^{calc} and t_{bi}^{meas} are the calculated and measured burst time for the i:th burst test, and n=151 is the total number of tests. The calculated burst time depends on the specific set of constant model parameters, $\mathbf{c}$, used for the calculation. The same principle applies to equation (19).

The parameter optimization was done by determining the set of model parameters $\mathbf{c}$ that resulted in a minimum value for ϕ. A Nelder-Mead [36] optimization algorithm, available in the MATLAB Optimization Toolbox [23], was used for this purpose. The vector $\mathbf{c}$ contained seven tuning factors for the creep and burst model parameters, for which the nominal values defined in Tables 2 and 3 were used as a starting point for optimization. Hence, all elements of $\mathbf{c}$ were tuning factors initially set to unity, and they changed moderately as the optimization proceeded.

The result of any optimization inevitably depends on how the loss function is defined. Here, we decided to consider *relative* rather than *absolute* deviations between calculated and measured results, since measured values for t_b and σ_b range over nearly two orders of magnitude. Moreover, the loss function defined by equation (17) contains relative differences for both t_b and σ_b, which means that the optimization will lead to a combined best fit with regard to both these parameters. No weights were applied to the two right-hand-side terms in equation (17), meaning that the relative differences of t_b and σ_b were considered equally important in the model parameter optimization. In this context, it should be remarked that the burst stress is a composite parameter that depends on both the overpressure of the sample and the burst hoop strain; see equation (A.5) in Appendix A. Hence, although the burst hoop strain does not explicitly appear in the loss function defined by equation (17), it is implicitly included as a target parameter in the optimization. Finally, we note that also the choice of vector norm for evaluating the relative differences in the loss function will affect the outcome of the parameter optimization [35]. We used the l^2-norm, since it is by far the most commonly used norm in parameter optimization. However, it is sensitive to outliers, and norms of lower order (or a combination of l^2 and a lower order norm) could possibly be used to reduce this sensitivity.

3 Results and discussion

The calibration of constant parameters in the cladding creep and burst models were done in three consecutive steps, where the first two steps were of preparatory nature:

1) Optimization of creep model parameters only. No analytical burst criterion was used in this step. Instead, the measured burst strain for each test was used as a criterion for cladding burst in the calculations. The applied loss function was $\phi = l^2\left(\mathbf{D}_r(t_b)\right)$, which means that the optimization considered only the time to burst. Sensitivity studies were also done to identify feasible creep model parameters for optimization: as mentioned in Section 2.2.3, only two parameters were found suitable.

2) Optimization of burst criterion parameters only. The calculations were done with fixed creep model parameters, as determined in Step 1). The applied loss function was $\phi = l^2\left(\mathbf{D}_r(\sigma_b)\right)$, i.e. the optimization considered only the burst stress.

3) Final optimization of the creep and burst model parameters simultaneously. The separately optimized parameters from Steps 1) and 2) were used as a starting point for the optimization, and the loss function defined by equation (17) was used.

The third step thus considered the interplay between the creep model and the burst criterion, and the calibration in this step was aimed to minimize relative differences in both burst time and burst stress between calculated and measured results. Only the results of the third step are presented and discussed below.

3.1 Optimized model parameters

3.1.1 Cladding creep deformation

The calibration resulted in a reduction of the coefficient A_c in equation (14) by a factor 0.709 for the α-phase and 0.771 for the β-phase. Hence, with reference to Table 2, the optimized values for A_c are 2.834×10^{-32} and 1.272×10^{-22} $\mathrm{s}^{-1}\mathrm{Pa}^{-n}$ for α- and β-phase material, respectively. As will be shown in section 3.2.1, this reduction of the calculated creep rate eliminates the bias in calculated time to burst. More precisely, the original creep model tended to underestimate the time to cladding burst, not only for the burst tests considered here, but also for integral-type LOCA simulation tests on high-burnup fuel rods [10]. In analyses of the latter tests with the original models, an ad-hoc reduction factor of 0.40 was applied to the calculated creep rate, α- and β-phase alike, to achieve reasonable agreement between calculated and measured burst times [10]. This large reduction factor may be due to effects of delayed gas flow in the high burnup fuel rods: due to the narrow or closed pellet-cladding gap that is typical for high-burnup LWR fuel rods, restrictions in the axial flow of gas from the rod plenum will reduce the rate of pressure-driven cladding distension in the ballooning region.

3.1.2 Cladding burst criterion

The optimized parameters for the cladding burst criterion in equation (16) are presented in Table 4. The burst hoop stress calculated with the optimized criterion is compared with the thresholds given by Rosinger's upper bound and best-estimate criteria in Figure 4. It is clear that the optimized criterion is very close to Rosinger's best-estimate criterion in the β-phase and mixed $(\alpha + \beta)$-phase regions, but that it gives significantly higher values for the burst hoop stress in the α-phase region, i.e. for temperatures below 1075 K.

Table 4: Constants used for the optimized burst stress criterion defined in equation (16).

Temperature region (K)	A_b (Pa)	B_b (K^{-1})	C_b (-)
873 to 1075	7.3757×10^{10}	5.9298×10^{-3}	5.888×10^{-4}
1075 to 1250	5.1513×10^{12}	9.8798×10^{-3}	5.888×10^{-4}
1250 to 1873	2.3301×10^{7}	3.4814×10^{-5}	5.888×10^{-4}

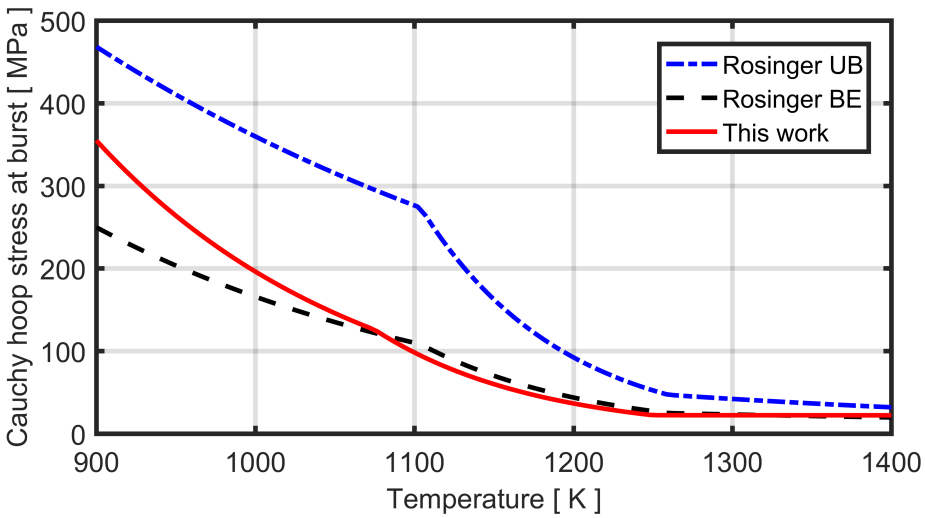

Figure 4: Cauchy hoop stress at burst, calculated for as-fabricated Zircaloy cladding ($x_{Met} = x_{Tot} = 0$) through Rosinger's upper bound (UB) and best-estimate (BE) correlations in equation (15) and the optimized correlation in equation (16). The model parameters are defined in Tables 3 and 4.

The stress thresholds presented in Figure 4 are calculated for Zircaloy cladding without any excess oxygen from high-temperature metal-steam reactions. Consequently, they cannot be readily compared to the burst stress data in Figure 1, since the test samples are oxidized to various degrees, depending on their dwell time at high temperature. However, in Figure 5, the optimized burst criterion is plotted versus temperature for two different excess oxygen concentrations, $x_{Met} = 0$ and $x_{Met} = 3 \times 10^{-4}$, and burst strain data for samples with a calculated oxygen concentration within this range at time of burst are included for comparison. More precisely, data from 132 samples are included in Figure 5, which corresponds to 87 % of the entire database described in Section 2.1. The peak calculated value of x_{Met} for any sample in the database is about 700 wppm; see Appendix B. From Figure 5, it is clear that the data for $0 < x_{Met} < 3 \times 10^{-4}$ are in reasonable agreement with the calculated burst stress for this range of x_{Met}, but the burst stress is generally underestimated for the KfK-88 data. This is further discussed below.

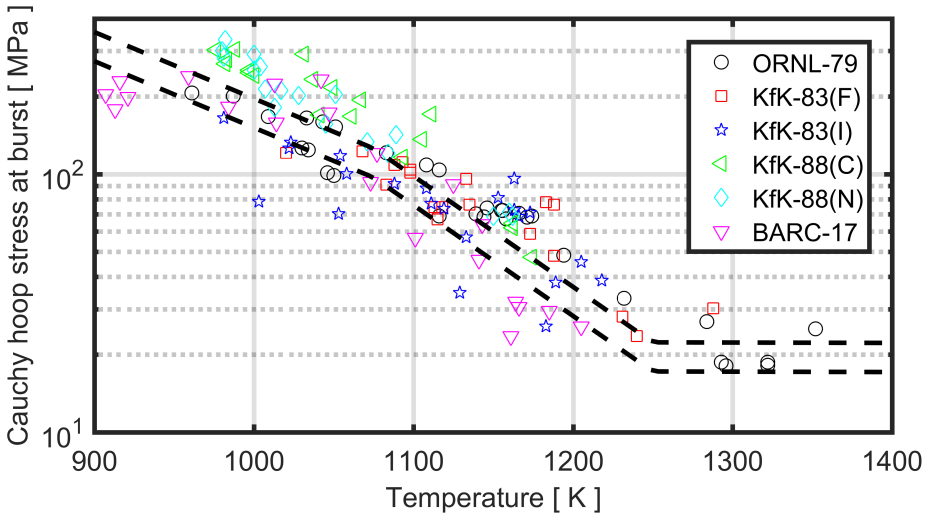

Figure 5: Burst hoop stress versus temperature, calculated through equation (16) for $x_{Met} = 0$ and $x_{Met} = 3 \times 10^{-4}$, in comparison with burst test data for 132 Zircaloy-4 samples with a calculated excess oxygen concentration within this range.

3.2 Model-data comparisons

3.2.1 Comparisons with the calibration database

Figures 6 to 9 show calculated time to cladding burst, burst temperature, burst hoop stress and burst hoop strain in comparison with measured results from the database used for model calibration. To illustrate the improvements made by calibrating the parameters in the creep model and the burst criterion, results calculated with the calibrated and original models are juxtaposed. Uncertainty bands, corresponding to $\pm 2\sigma$ differences between calculated and measured results, are included in the figures. The standard deviations, $\sigma(\mathbf{D}_r)$, and mean values, $\bar{\mathbf{D}}_r$, for the relative differences, $\mathbf{D}_r$, between calculated and measured results are given in Table 5 for each parameter of interest. The standard deviations are measures of the dispersion of the relative differences between calculated and measured results, whereas the mean values are measures of the bias in the models: $\bar{\mathbf{D}}_r < 0$ means that the models generally underestimate the parameter, while $\bar{\mathbf{D}}_r = 0$ is the best possible fit. From Table 5, it is clear that the calibration has reduced the bias by about an order of magnitude for all parameters except the burst strain. Also the dispersion has been reduced as a result of the calibration, most notably for the burst strain. The improved overall performance of the models is clear from the bottom line of Table 5, which shows the mean values and standard deviations for the relative differences between calculated and measured results for the four different parameters combined. The statistical measures for the uncertainty in calculated burst times, temperatures, stresses and strains that are presented in Table 5 are valuable for assessing uncertainties in future LOCA safety analyses with the calibrated models.

The improved performance of the models is also evident from Figures 6 to 9. In particular, from Figures 6 - 7 and Table 5, it is clear that the burst time and burst temperature are generally reproduced with high accuracy over the entire time/temperature range spanned by the database. The calculated time to burst is in most cases controlled by the creep model: the burst criterion is far less important. The reason is that cladding burst normally occurs when

stable creep deformation to a hoop strain of 20-40 % suddenly turns unstable as a result of the exponential relationship between cladding hoop stress and strain; see equation (A.5) in Appendix A. Under these conditions, the exact burst stress/strain threshold postulated by the cladding burst criterion has very little impact on the calculated time to burst, since the ballooning-type deformation beyond the stable-to-unstable transition point is very fast. In fact, investigators have reported that a simple fixed threshold for the hoop logarithmic strain of about 35 % works well as a cladding burst criterion for LOCA, provided that only the time to burst is of interest [12]. However, prediction of burst strain is usually required in LOCA safety analysis, since the burst strain is important for assessing the risk for coolant flow blockage and loss of long-term coolability, and also for calculating post-burst oxidation and embrittlement of the ballooned cladding. Definite thresholds for cladding strain, whether they are fixed or defined as functions of temperature and/or other parameters, are for this reason rarely used as burst criteria in LOCA safety analyses [37].

Table 5: Mean values and standard deviations for the relative differences between calculated and measured results, $\mathbf{D}_r$. Statistical measures are given for both the optimized and original models.

	Mean value, $\bar{\mathbf{D}}_r$		Standard deviation, $\sigma(\mathbf{D}_r)$	
Parameter:	Optimized	Original	Optimized	Original
Burst time, t_b	-0.0049	-0.0414	0.0667	0.0769
Burst temperature, T_b	-0.0012	-0.0200	0.0330	0.0401
Burst hoop stress, σ_b	-0.0291	-0.1134	0.1714	0.2367
Burst hoop strain, ε_b	-0.1532	-0.3090	0.2435	0.3888
Average, all parameters	-0.0471	-0.1210	0.1531	0.2310

While optimization of the parameters in the burst stress criterion had only a minor effect on the calculated time to burst, it significantly improved the accuracy of the calculated burst stress and burst strain. From Figure 8, it is evident that the original criterion systematically underestimated burst stresses below 40 MPa. This tendency is eliminated with the optimized criterion. The improvement is mainly a result of the modified formulation for the effect of cladding oxygen uptake, i.e. x_{Tot} versus x_{Met} in equations (15) and (16). The optimized burst criterion calculates a weaker effect of oxygen uptake from cladding metal-steam reactions than Rosinger's original criterion [26].

Also, it is clear from Figure 9 that the optimized creep and burst models reproduce the measured cladding burst hoop strain with much higher fidelity than the original models. In particular, the original models significantly underestimated the burst strains for a fairly large number of tests, conducted in several experimental series. This is not the case for the optimized models. Yet, the optimized models tend to underestimate the burst strains; see Table 5. Especially the burst strains measured in the KfK-88 experiments are underestimated: hoop logarithmic strains up to 73 % were observed in these experiments, while burst strains calculated with the optimized models barely go beyond 50 %. As mentioned in Section 2.1, there is a very clear correlation between the hoop strain at burst and the uniformity of the temperature along the cladding circumference during the test. The cladding samples used in the KfK-88 experiments were heated both from the inside and from the outside [19], which together with slow heating (1.1 Ks^{-1}) lead to a nearly uniform temperature along the cladding circumference, and hence, to exceptionally high burst strains; see Figure 2. The circumferential (azimuthal) temperature difference was less than 10 K in the KfK-88 tests [19]. Other heating methods and higher heating rates generally produce

larger circumferential temperature differences in the cladding samples, which results in lower burst strains. Moreover, the magnitude of the circumferential temperature difference usually varies from one sample to another, which gives a large spread in the burst strain data.

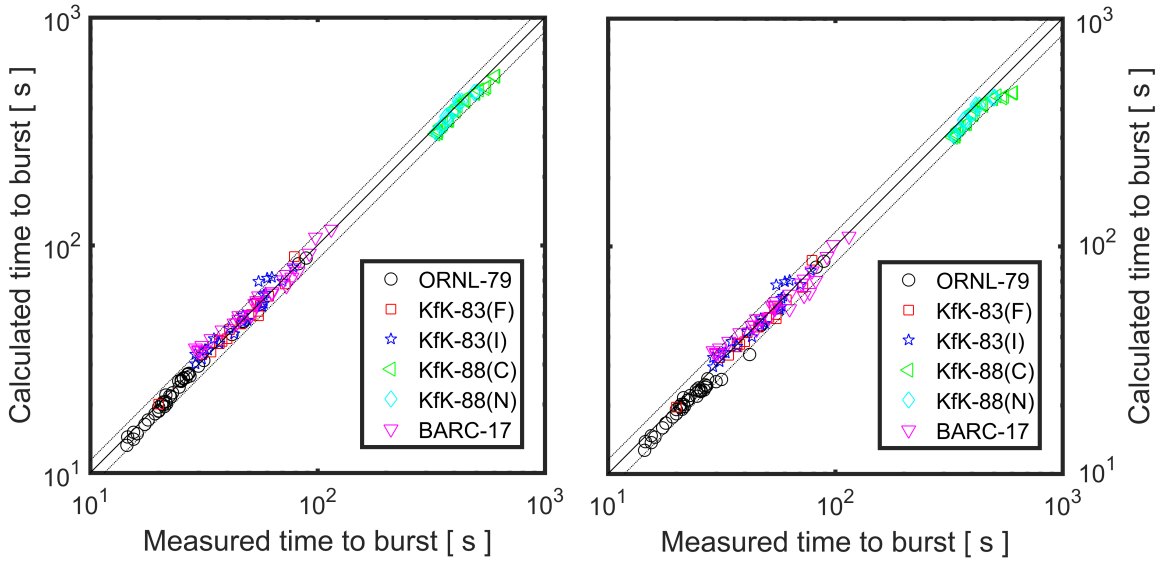

Figure 6: Calculated versus measured time to cladding burst. Calibrated models to the left, original models to the right. The dotted lines correspond to a $\pm 2\sigma$ uncertainty band for relative difference between calculated and measured t_b; see Table 5.

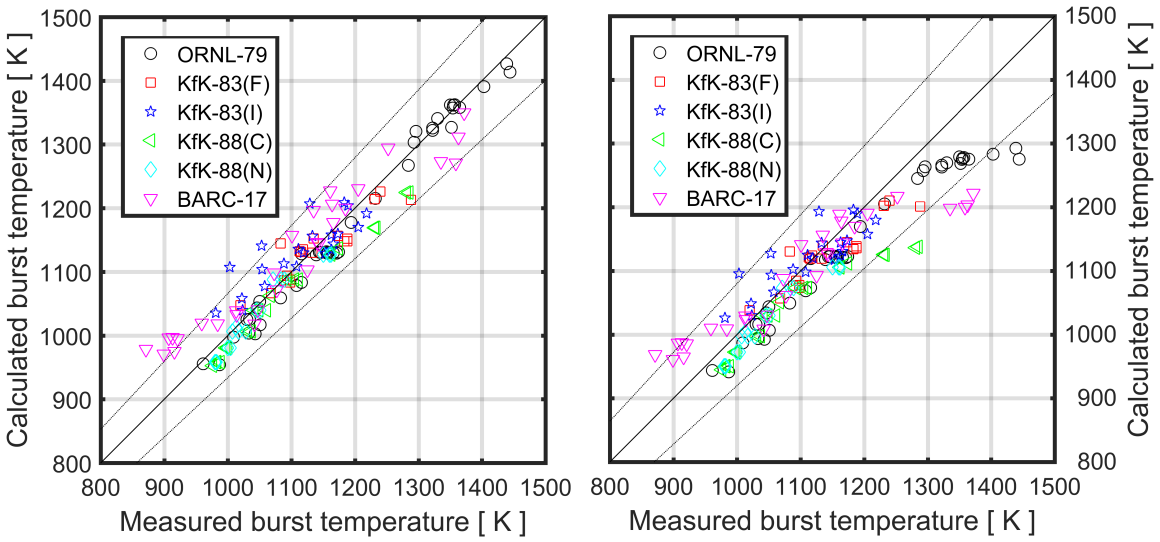

Figure 7: Calculated versus measured burst temperature. Calibrated models to the left, original models to the right. The dotted lines correspond to a $\pm 2\sigma$ uncertainty band for relative difference between calculated and measured T_b; see Table 5.

In this report, we consider burst tests that are conducted on a single fuel rod or cladding sample at a time. Irrespective of the heating method, these tests produce lower circumferential temperature differences than those expected in a light water reactor fuel assembly under LOCA. More specifically, multi-rod tests, performed on fuel bundles with 20-50 instrumented test rods, show that the cladding circumferential temperature differences in the

test rods within the bundle are typically 20-70 K in simulated LOCA conditions [21, 38]. As a consequence, cladding hoop logarithmic strains at burst rarely exceed 45 % in these bundle tests [21, 38]. Hence, the fact that our optimized models underestimate the exceptionally large cladding burst strains observed in the KfK-88 single rod experiments should not be considered as a problem: the models are intended primarily for simulating the fuel rod behaviour under postulated LWR LOCA conditions, i.e. the behaviour of fuel rods that are part of a fuel assembly.

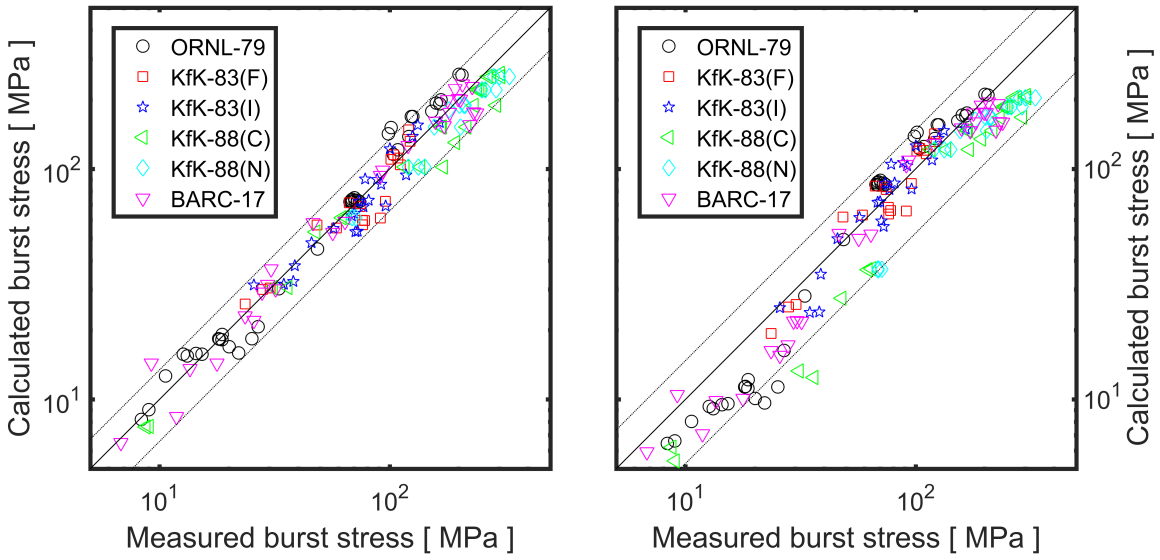

Figure 8: Calculated versus measured burst hoop stress (Cauchy). Calibrated models to the left, original models to the right. The dotted lines correspond to a $\pm 2\sigma$ uncertainty band for relative difference between calculated and measured σ_b; see Table 5.

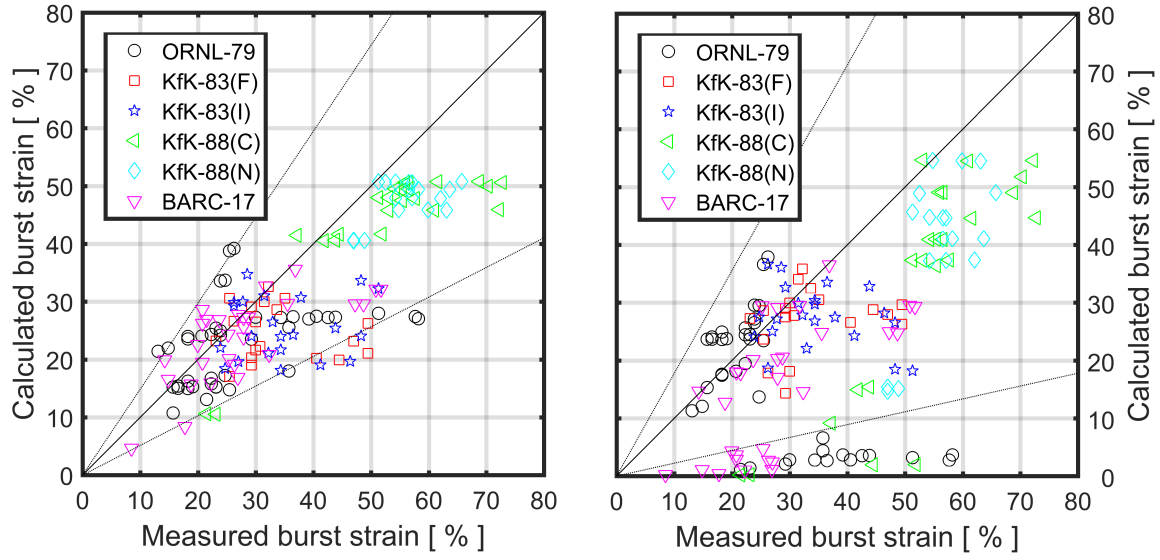

Figure 9: Calculated versus measured burst hoop strain (logarithmic). Calibrated models to the left, original models to the right. The dotted lines correspond to a $\pm 2\sigma$ uncertainty band for relative difference between calculated and measured ε_b; see Table 5.

More detailed comparisons of calculated and measured results are presented in Appendix B, where relative differences between the calculated and measured time to cladding burst and

cladding hoop stress at burst are plotted as functions of six selected parameters. The aim is to identify trends with regard to these parameters, i.e. whether there are tendencies for the models to underestimate or overestimate the experimental data for certain parameter ranges. In summary, the following conclusions can be drawn from the model-data comparisons in Appendix B:

- When looked upon individually, some test series reveal trends with regard to specific parameters, such as temperature or heating rate. An example is the BARC-17 test series, where the relative differences between calculated and measured time to burst seem to decrease with increasing burst temperature. The trend is clear at least at low temperature ($<$1000 K). However, when *all* test series are considered, or a wider parameter range is assessed, it is difficult to discern any clear trends in the model-data comparisons. In conclusion, one should be careful not to rely on results from a single test series for model calibration, neither should the models be applied to conditions not covered by the database used for their calibration.
- The calculated time to burst is within $\pm$10 % of the measured value for most tests in the database. Outliers, for which the burst time is overestimated by more than 10 %, belong almost exclusively to the BARC-17 and KfK-83(I) test series. For the former, the outliers are characterized by very low burst temperature ($<$930 K). For the latter, effects of sample pre-irradiation on the cladding creep deformation may be responsible for the model-data differences. More specifically, the model-data comparisons suggest that the cladding creep at low temperature (pure α-phase) for the pre-irradiated samples is faster than calculated by the models. Possible effects of pre-irradiation on cladding high-temperature creep and burst are discussed in Sections 3.2.2 and 4.2.
- The KfK-88 test were done with slow heating (1.1 Ks^{-1}), which resulted in much longer time to cladding burst than for other test series in the database. Notwithstanding the slow heating, the burst times and burst hoop stresses for these tests are reproduced with fair accuracy by the models: the burst times are only slightly underestimated, while the deviations for the burst stresses are somewhat larger. These deviations are linked to the underestimated burst strains for the KfK-88 tests; see Figure 9.

3.2.2 Comparisons with data for Zircaloy-2 and ZIRLO

As noted in our previous assessment of cladding high-temperature burst test data [7], there are few test series available in the open literature that are reported in sufficient detail to allow simulations of individual tests, and hence, to allow one-to-one comparisons of calculated and measured results. Most of these test series are included in the calibration database; see Section A.2 in Appendix A. However, in the following, results calculated with the optimized models are compared with measured data from three additional burst test series. Although they are limited to a handful tests each and carried out under specific and almost identical testing conditions, the additional series are deemed valuable for independent validation of the optimized models: the tests are documented in detail, they were done on cladding materials other than Zircaloy-4 and finally, they were partly done on irradiated cladding materials that were carefully characterized before testing. Hence, these burst test

series allow comparisons to be made between different cladding alloys and between fresh and irradiated cladding materials.

The testing conditions in the three test series were very similar: all tests were conducted in steam and with external heating. All samples were brought to an initial temperature of 573 K, pressurized to a pre-defined overpressure (mostly 8.28 MPa) at this temperature, and then heated to burst with a constant heating rate of 5 Ks^{-1}. The internal pressure varied moderately during the tests, due to gradually increasing sample temperature and internal volume. The test series are described in further detail in Section A.3, Appendix A.

The first test series included seven burst tests on Zircaloy-2 cladding material, carried out at the Argonne National Laboratory (ANL), USA [39]. Four tests were done on fresh (as-fabricated) cladding material, whereas three tests were done on samples taken from discharged 9×9-type boiling water reactor (BWR) fuel rods with a burnup of 56-57 $\mathrm{MWd(kgU)}^{-1}$. These samples were moderately corroded, with an external oxide layer of about 10 μm and a hydrogen concentration around 70 wppm [39]. All tests were done under identical conditions to allow comparisons between the samples. The second test series included twenty-two burst tests on fresh ZIRLO cladding material of the first generation, carried out at ANL with testing conditions that were very similar to those used previously by ANL, as described above [40]. The third test series included six burst tests on irradiated ZIRLO cladding material of the first generation, carried out by Studsvik Nuclear, Sweden [41]. The material was sampled from 17×17-type pressurized water reactor (PWR) fuel rods, which had been irradiated to rod average burnups of 55 and 68 $\mathrm{MWd(kgU)}^{-1}$. The testing conditions were very similar to those used by ANL.

The aforementioned tests were simulated with the optimized models for cladding high-temperature creep and burst in `FRAPTRAN-QT-1.5`. The estimated or measured hydrogen concentration for each sample was used as input to the calculations. In this context, we recall from Section 2.2.2 that the hydrogen concentration affects the cladding phase composition. The calculated results are compared with measured data from [39–41] in Figures 10 and 11.

Figure 10 shows that the time to cladding burst and the burst temperature are calculated with fair accuracy for the ANL-08 tests, both for the fresh (F) and irradiated (I) Zircaloy-2 samples. The calculated burst times and temperatures are very similar for all these tests, and the measured data show no significant differences between fresh and pre-irradiated samples. For the ZIRLO samples, the burst times and burst temperatures are overestimated. On average, the burst time is overestimated by 6 % for the twenty-two ANL-10 tests on fresh ZIRLO samples and by 17 % for the six Studsvik tests on pre-irradiated samples. The results suggest that the creep rate of ZIRLO cladding is slightly higher than that of Zircaloys, and that the creep rate is increased by effects caused by pre-irradiation; these effects are further discussed in Section 3.3 below. It is recommended to increase the coefficients A_c in the creep model given by equation (14) by 8 %, when applying it to ZIRLO cladding: this number corresponds to the average overestimation of burst time for all ZIRLO samples (fresh and pre-irradiated) in Figure 10.

Figure 11 shows a fair agreement between calculated and measured burst hoop stress and strain for all the ANL and Studsvik tests: the agreement is comparable to that for tests in the calibration database. The data show no significant differences between fresh and pre-irradiated samples. In fact, the investigators at ANL concluded that pre-irradiation to

high burnup (56-57 MWd(kgU)$^{-1}$) for the Zircaloy-2 samples had little effect on cladding burst temperatures and burst strains. They reported that the primary differences between the fresh and pre-irradiated test rods were in the pre-burst bending (larger for fresh rods), the axial extent of the ballooned region (larger for fresh rods), and the shape of the burst opening (dog-bone for fresh rods, oval for pre-irradiated) [39].

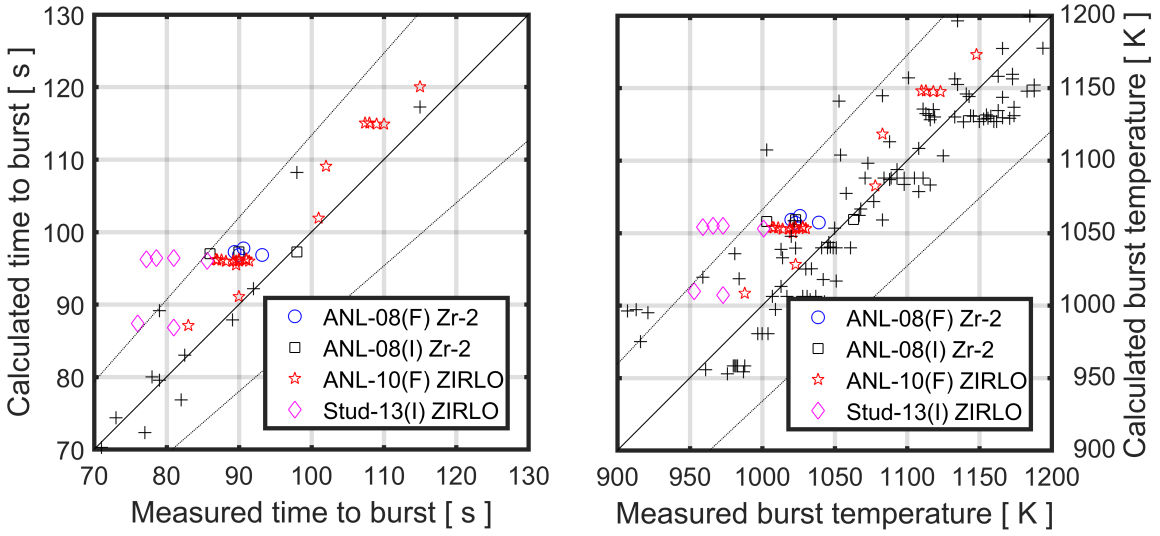

Figure 10: Calculated versus measured time to cladding burst (left) and burst temperature (right). Black crosses represent data from the calibration database, while symbols in colour are the ANL-08 [39], ANL-10 [40] and Studsvik [41] tests. The dotted lines correspond to a $\pm 2\sigma$ uncertainty band for relative difference between calculated and measured results; see Table 5.

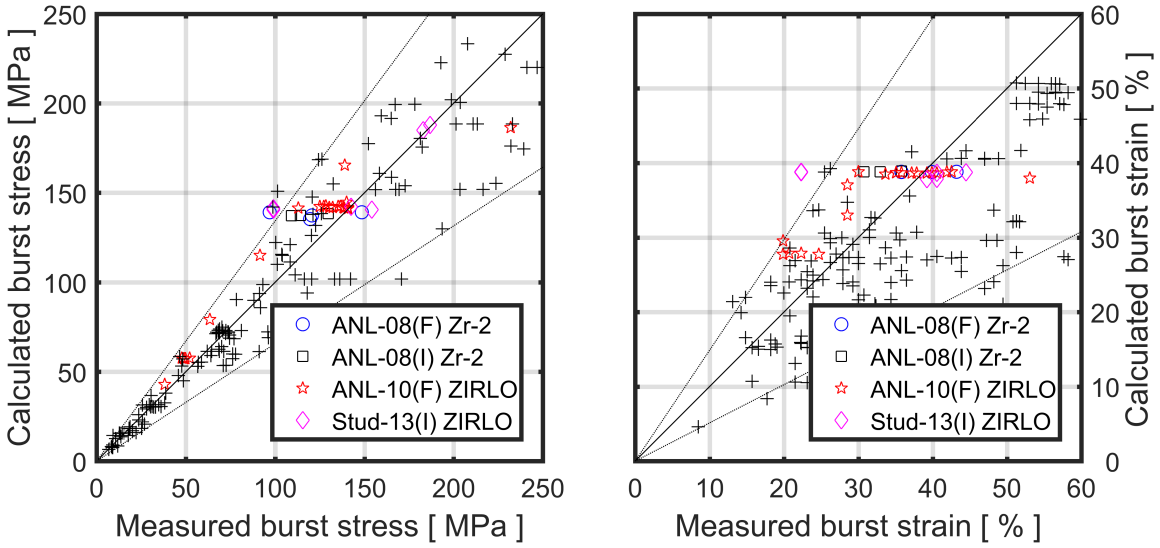

Figure 11: Calculated versus measured burst hoop Cauchy stress (left) and logarithmic hoop strain (right). Black crosses represent data from the calibration database, while symbols in colour are the ANL-08 [39], ANL-10 [40] and Studsvik [41] tests. The dotted lines correspond to a $\pm 2\sigma$ uncertainty band for relative difference between calculated and measured results; see Table 5.

3.3 Effects of pre-irradiation

The database used for model calibration in this report contains burst test conducted mainly on as-fabricated Zircaloy-4 cladding. More specifically, only 22 of the 151 considered tests were done on pre-irradiated samples. The latter tests were done in the FR2 research reactor, Germany, on UO_2 test rods with fuel burnups ranging from 2.5 to 35 MWd(kgU)$^{-1}$ [18]; see the KfK-83(I) test series in Section A.2.3 in Appendix A. Unfortunately, there is virtually no information available on the pre-test conditions of these test rods, e.g. regarding the extent of cladding corrosion. Considering the wide burnup span, one may expect a fairly large variation among the samples. Nevertheless, our model-data comparisons in Section 3.2.1 and Appendix B show that there is a tendency for the calibrated models to overestimate the burst time and burst temperature for most of the pre-irradiated KfK-83 samples, especially for those that failed at low temperature. A similar tendency was also observed in Section 3.2.2 for six pre-irradiated ZIRLO cladding samples in the Studsvik-13 test series.

Although the observed tendencies are rather weak and the number of pre-irradiated samples is limited, the possible effects of pre-irradiation and in-reactor service life on cladding high-temperature ballooning and burst under LOCA deserve attention. In principle, these effects may arise from radiation induced damage to the cladding metal and/or from cladding corrosion. Radiation damage in zirconium alloy cladding tubes is caused mainly by incident neutrons with high energy, which inflict microstructural damage to the material through knockout and recoil processes in the metal lattice [42]. The resulting material damage is in the form of point defects, small dislocations loops, short line dislocations and dislocation entanglements. At normal operating temperatures for the cladding, these defects remain in the material and raise the yield strength and reduce the ductility of zirconium alloys by hindering dislocation movements, which is the dominant mechanism responsible for plastic deformation and creep in metals. However, current understanding is that these defects are rapidly annealed at temperatures reached already in the initial phase of a LWR LOCA, and consequently, that they have very little effect on the cladding high-temperature ballooning and burst behaviour [43–45].

Cladding corrosion, on the other hand, may affect the ballooning and burst behaviour in several ways. Firstly, the corrosion leads to formation of an oxide layer at the cladding outer surface. The oxide layer is brittle, and studies have shown that cracks form easily in the oxide at only about 0.2-0.3 % plastic hoop strain of the underlying metal [46]. Hence, at this strain level, the oxide layer looses its load-bearing capacity. Moreover, since the cladding corrosion is non-uniform, the oxide formation may cause localization effects, i.e. deviations from axial symmetry, that lead to failure of the cladding at low overall hoop strain [47]. Oxygen may also diffuse from the oxide layer into the cladding metal, when the temperature increases to more than about 1000 K. As shown in Sections 2.2.2-2.2.4, excess oxygen in the cladding metal affects most aspects of the high-temperature behaviour. The detrimental effects of a pre-existing oxide layer on cladding ballooning and burst during LOCA have been demonstrated experimentally by Kim and co-workers [48]. They carried out high-temperature burst tests on Zircaloy-4 cladding in three different conditions: as-fabricated, pre-oxidized and pre-charged with hydrogen. The results showed that the pre-oxidized samples, with either 20 or 50 μm thick oxide layer, had significantly lower hoop burst strain than the as-fabricated samples [48].

Secondly, the corrosion reactions produce hydrogen. Part of the produced hydrogen enters into the cladding metal, where it migrates by thermo-diffusion towards cold regions of the cladding. During normal reactor operation, hydrogen will thus accumulate close to the comparatively cold outer surface of the cladding tube. When the local hydrogen concentration exceeds the terminal solid solubility, zirconium hydrides precipitate. Under a LOCA, these hydrides are dissolved as the cladding temperature rises and the hydrogen solubility increases [49]. Hydrogen in solid solution affects the high-temperature behaviour of zirconium alloys in many ways. For example, hydrogen is known to significantly reduce the transition temperature from α-phase to mixed $(\alpha + \beta)$-phase material, and to some extent also the transition temperature from mixed $(\alpha + \beta)$- to β-phase [44]. This phenomenon, which is considered in our phase transformation model [6], indirectly affects the cladding high-temperature creep and burst behaviour, since this behaviour depends on the phase composition of the material. However, Brachet and co-workers [44] studied the effects of hydrogen on cladding mechanical behavior at LOCA-relevant temperatures and concluded that the effects cannot be explained solely by the hydrogen-induced shift of the α/β phase transformation temperatures, but that hydrogen modifies also the creep and burst behaviour, especially in the α-phase and lower $(\alpha + \beta)$-phase temperature range.

Hydrogen is also known to affect the solubility and diffusivity of oxygen in zirconium alloys at high temperature, which leads to a hydrogen-dependence for the oxygen distribution in the overheated cladding. This has been found important for the resistance to thermal shock under quenching (re-wetting) and the so-called post-quench ductility (PQD), i.e. the ductility retained by the cladding after a postulated LOCA terminated by quenching [39]. With the aim to investigate the effects of hydrogen on thermal shock resistance and post-quench ductility, a fairly large number of LOCA-simulation experiments have been done on un-irradiated zirconium-base cladding materials that have been charged with hydrogen before testing [40, 48, 50–52]. These experiments were typically conducted by heating cladding samples with an internal overpressure of about 5 MPa in steam environment to a target temperature of 1400-1500 K, holding the sample at this temperature a few minutes for isothermal oxidation, then slowly cooling the sample to around 1000 K, after which it was rapidly cooled by quenching in water. Various degrees of axial constraint was applied to the sample under quenching, to investigate the importance of this parameter to the risk for brittle fracture under conditions of thermal shock. After the simulated LOCA, the samples were usually mechanically tested for post-quench ductility and subjected to metallographic investigations. The majority of these tests resulted in cladding ballooning and burst during the initial heating phase, but since the experiments were intended primarily to study how hydrogen affects the risk for cladding brittle fracture during and after quenching, very few data related to the high-temperature ballooning and burst behaviour have been presented from these studies: a notable exception is [40], which contains a fairly complete description of the entire test sequence.

Nevertheless, available data from the aforementioned LOCA simulation tests on hydrogen-charged cladding generally show that both burst temperature, T_b, and burst hoop strain, ε_b, decrease with increasing hydrogen concentration. This is illustrated by data from [51] in Figures 12 and 13. Similar results for more limited data sets are presented in [40, 48, 52]. The studies consistently show that both T_b and ε_b decrease with increasing hydrogen concentrations, but that fairly high concentrations are needed to yield significant differences in relation to the typical scatter observed in burst data. By comparing the results of burst tests on hydrogen-charged cladding samples versus tests on pre-irradiated samples, Nagase

and co-workers [53, 54] concluded that the cladding hydrogen concentration is the most important burnup-related factor for the high-temperature burst behaviour of LWR fuel rods: effects of other high-burnup characteristics are generally small.

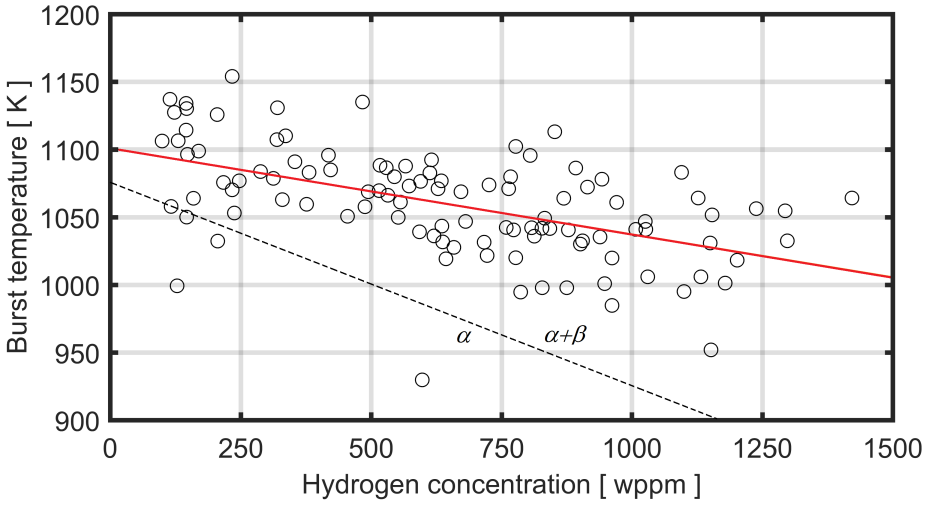

Figure 12: Observed dependence of cladding pre-test hydrogen concentration on burst temperature during LOCA-simulation tests on hydrogen-charged Zircaloy-4 samples [51]. The full red line is a best linear fit to the data. The effect of hydrogen on the α- to $(\alpha + \beta)$-phase transition is indicated by the dashed black line [6].

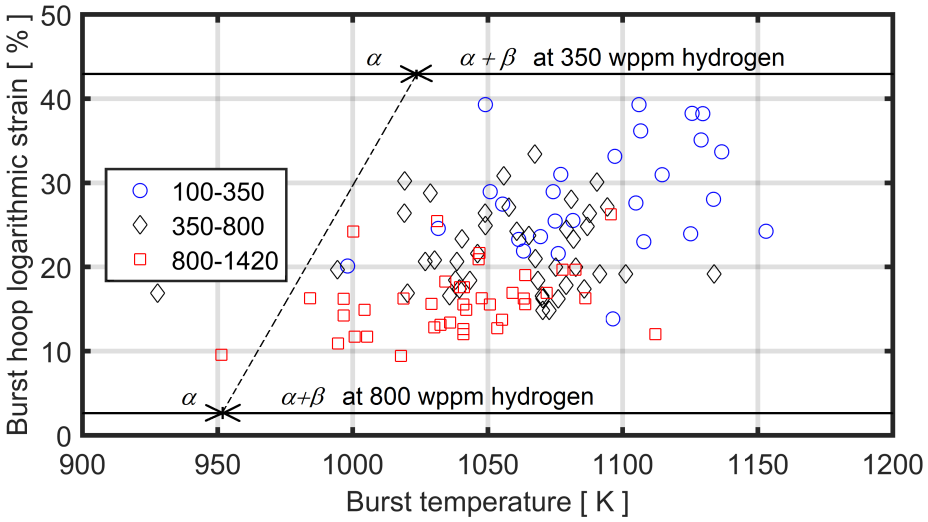

Figure 13: Observed effect of cladding pre-test hydrogen concentration (wppm, as indicated in the legend) on hoop logarithmic strain at burst during LOCA-simulation test on hydrogen-charged Zircaloy-4 samples [51]. The effect of hydrogen on the α- to $(\alpha + \beta)$-phase transition is indicated by the dashed line [6].

4 Summary, conclusions and outlook

4.1 Summary and conclusions

In earlier projects for the Swedish Radiation Safety Authority, models for high-temperature behaviour of zirconium-base cladding to light water reactor fuel rods, pertinent to conditions expected in loss-of-coolant accidents, have been developed and implemented in the `FRAPTRAN-QT-1.5` computer program [3]. Analyses of integral-type LOCA simulation experiments [10] as well as high-temperature cladding burst tests [7] with these models have revealed a need for integral calibration of the models: until now, the models have been calibrated one at a time against separate effect tests. In the work presented here, an integral calibration was performed by optimizing selected model parameters against a primary database with 151 high-temperature burst tests on Zircaloy-4 cladding. The objective was to improve the performance of the models with regard to prediction of time to cladding burst, burst temperature, burst stress and burst strain over a wide range of accident conditions. After calibration, the models were assessed against additional burst test data on Zircaloy-2 and ZIRLO cladding, in order to test and verify their applicability to these materials.

All tests considered in this report were single-rod burst tests, conducted in steam at or near atmospheric pressure. The steam supply was sufficient to feed the metal-steam reactions (no steam starvation). Different heating methods were used in the considered tests, most of which were conducted out-of-reactor. Table 6 summarizes the testing conditions, cladding designs and cladding pre-test conditions covered by the tests. Information on the considered tests was compiled from open literature sources, part of which have been assessed in earlier work [7]. The tests were selected based on availability of information: the considered tests were sufficiently documented to be simulated with exactitude and to allow reliable comparisons of calculated versus measured burst time, burst temperature and burst hoop strain. These comparisons provide statistical measures for the uncertainty in calculated properties, which are valuable for assessing uncertainties in future LOCA safety analyses with the calibrated models. Analysis of the reliability (confidence) of the statistical measures is beyond the scope of this report.

Table 6: Summary of testing conditions, cladding designs and cladding pre-test conditions covered by the burst test data considered in this report.

Testing conditions		Range
Environment	[-]	Steam
Rod internal overpressure, ΔP	[MPa]	0.3 - 20.8
Heating rate, $\dot{T}$	[Ks^{-1}]	1.1 - 30.6
Burst temperature, T_b	[K]	871 - 1444
Burst hoop logarithmic strain, ε_b	[%]	8.5 - 72.8
Cladding design and pre-test conditions		
Outer diameter, D_o	[mm]	9.50 - 15.20
Wall thickness, W_o	[mm]	0.400 - 0.725
Oxide layer thickness	[μm]	0 - 30
Hydrogen concentration	[wppm]	10 - 290

In a first step, seven constant model parameters were calibrated against the primary database with Zircaloy-4 burst tests by use of a Nelder-Mead optimization algorithm. The optimization was done, such that the l^2-norms of relative differences between calculated and measured values for burst time and burst stress were minimized. As indicated by the reduced standard deviations and mean values for the relative differences between calculated and measured results presented in Table 5, the calibration significantly improved the models' capacity to reproduce burst times, temperatures, stresses and strains for the considered tests on Zircaloy-4. Systematic errors in the calculated burst time, burst temperature and burst hoop stress were practically eliminated. The fact that the models still underestimate burst strains in the database is not a problem, since the models are intended primarily for analysing the behaviour of fuel rods that are part of a fuel assembly: it is well known that, as a result of circumferential temperature differences and other deviations from axial symmetry, fuel rods within a fuel assembly generally exhibit lower burst strains under LOCA than those measured in single-rod burst tests, where the conditions are more symmetric.

In a second step, the optimized models were assessed against three series of burst tests on Zircaloy-2 and ZIRLO cladding materials. The purpose was to test the applicability of the models to these materials, and also to investigate possible effects of irradiation during in-reactor service on the cladding burst behaviour: 9 of the 35 tests considered in the second step were conducted on well-characterized cladding materials sampled from high-burnup (56-68 MWd(kgU)$^{-1}$ rod average) BWR and PWR fuel rods. Although the number of tests is limited, the model-data comparisons suggest that the models, calibrated in the first step against Zircaloy-4 data only, are applicable to fresh and pre-irradiated Zircaloy-2 cladding without modifications. For ZIRLO, the models tend to overestimate the burst time and burst temperature, in particular for pre-irradiated cladding. As a tentative remedy to eliminate this bias, the calculated high-temperature creep rate of ZIRLO is increased by a factor of 1.08 with regard to the calibrated model for Zircaloy-4 in `FRAPTRAN-QT-1.5` [5].

A more rigorous calibration of the models against experiments on ZIRLO is desirable, but unfortunately, the amount of useful experimental data for other cladding materials than Zircaloy-4 is currently very limited in the open literature. A thorough calibration effort, similar to that presented in this report, is for the time being impracticable for other cladding materials than Zircaloy-4. As of today, `FRAPTRAN-QT-1.5` contains models for the high-temperature behaviour of two groups of cladding materials: Zircaloys and Zr1%NbO-alloys [5]. Models for the first group, which includes Zircaloy-2, Zircaloy-4 and ZIRLO, have been fairly well validated against available data, as presented in this report. Models for the second group, which includes the M5 and E110 cladding materials, have been validated model-by-model against results from separate effect tests. However, they are still awaiting integral validation in `FRAPTRAN-QT-1.5`.

4.2 Outlook

Integral validation and calibration of models for the high-temperature behaviour of Zr1%-NbO-type cladding materials in `FRAPTRAN-QT-1.5` is left for the future, due to the current scarcity of experimental data for these materials in the open literature. The data at hand suggest significant differences in high-temperature behaviour between Zr1%NbO-alloys and Zircaloys, which means that additional data, specifically for the Zr1%NbO-type cladding materials, are essential for model validation and calibration.

As mentioned in Section 3.3, the data currently available in open literature consistently show detrimental effects of hydrogen on cladding ballooning and burst under simulated LOCA conditions. However, there are significant differences in the reported results, and more importantly, the observed effects are not properly understood or explained. Some investigators [44, 55] have proposed empirically based burst criteria, in which the burst stress is correlated not only to the cladding oxygen concentration, as in equation (16), but also to the cladding hydrogen concentration. These empirical correlations are supported by limited sets of experimental data, and their consistency with other data sources is unclear. Hence, a thorough analysis of theoretical work and data for hydrogen effects on cladding high temperature creep deformation and burst, including empirical burst criteria proposed for considering hydrogen effects, is justified. This subject is an area of current research, and the experimental database is constantly expanding.

In connection with such a study, it is also recommended to critically assess the method used by Rosinger [26] for considering the effect of oxygen (in our case oxygen and hydrogen) on the phase transformation temperatures, when calculating the cladding high-temperature creep rate. More precisely, Rosinger used the concept of a homologous temperature when calculating the creep rate in materials with different concentrations of excess oxygen. The concept implies that the creep rate of a material with high oxygen concentration at high temperature is assumed to be the same as that for a material with low oxygen at lower temperature [26]. This is possibly a more physically-based method than the empirical creep rate reduction factor for oxygen used in our creep model today; see equation (14). Moreover, the method is easy to extend, such that effects of both oxygen and hydrogen on the creep rate can be considered.

Acknowledgements

The work was funded by the Swedish Radiation Safety Authority (SSM) under research contract number SSM 2018-4296. Anna Alvestav at SSM is gratefully acknowledged for initiating the project and for providing helpful feedback to the work.

References

[1] P. Van Uffelen, J. Hales, W. Li, G. Rossiter, and R. Williamson. A review of fuel performance modelling. *J. Nucl. Mater.*, 516:373–412, 2019.

[2] Nuclear fuel behaviour in loss-of-coolant (LOCA) conditions. Report NEA No. 6846, OECD Nuclear Energy Agency, Paris, France, 2009.

[3] L. O. Jernkvist and A. R. Massih. Improving the FRAPTRAN program for fuel rod LOCA analyses by novel models and assessment of recent data. Annex II, pp 381-451, IAEA-TECDOC-1889, International Atomic Energy Agency, Vienna, Austria, 2019.

[4] K. J. Geelhood, W.G. Luscher, and J. M. Cuta. FRAPTRAN-1.5: A computer code for the transient analysis of oxide fuel rods. Report NUREC/CR-7023, Vol.1 Rev.1, U.S. Nuclear Regulatory Commission, Washington DC, USA, 2014.

[5] L. O. Jernkvist. Extended models in the FRAPTRAN-QT-1.5 program. Report TR20-004V1, Quantum Technologies AB, Uppsala, Sweden, 2020.

[6] A. R. Massih and L. O. Jernkvist. Modeling alpha-beta phase transformation kinetics in Zr-base alloys. Memo PM19-008V2, Quantum Technologies AB, Uppsala, Sweden, 2019.

[7] A. R. Massih and L. O. Jernkvist. Assessment of data and criteria for cladding burst in loss-of-coolant accidents. Research report 2015:46, Swedish Radiation Safety Authority, Stockholm, Sweden, 2015.

[8] T. Manngård, A. Massih, and J. O. Stengård. Evaluation of the Halden IFA-650 loss-of-coolant accident experiments 2, 3 and 4. Research report 2014:18, Swedish Radiation Safety Authority (SSM), Stockholm, Sweden, 2014.

[9] T. Manngård and J. O. Stengård. Evaluation of the Halden IFA-650 loss-of-coolant accident experiments 5, 6 and 7. Research report 2014:19, Swedish Radiation Safety Authority (SSM), Stockholm, Sweden, 2014.

[10] L. O. Jernkvist. Computational assessment of LOCA simulation tests on high burnup fuel rods in Halden and Studsvik. Report 2017:12, Swedish Radiation Safety Authority, Stockholm, Sweden, 2017.

[11] J. Karlsson et al. Modeling out-of-pile LOCA tests on high burnup fuel rods. Results of fourth SCIP modeling workshop. In *Reactor Fuel Performance 2018 (TopFuel-2018)*, Prague, Czech Republic, Sept. 30 - Oct. 4, 2018. European Nuclear Society.

[12] V. Di Marcello, A. Schubert, J. van de Laar, and P. Van Uffelen. The TRANSURANUS mechanical model for large strain analysis. *Nucl. Engng. Des.*, 276:19–29, 2014.

[13] T. K. Sawarn, S. Banerjee, S. S. Sheelvantra, J. L. Singh, and V. Bhasin. Study of clad ballooning and rupture behaviour of Indian PHWR fuel pins under transient heating condition in steam environment. *J. Nucl. Mater.*, 495:332–342, 2017.

[14] R. H. Chapman, J. L. Crowley, A. W. Longest, and G. Hofmann. Zirconium cladding deformation in a steam environment with transient heating. In *Zirconium in the Nuclear Industry: Fourth Conference*, volume ASTM STP 681, pages 393–408. American Society for Testing and Materials, 1979.

[15] R. H. Chapman, J. L. Crowley, A. W. Longest, and E. G. Sewell. Effect of creep time and heating rate on deformation of Zircaloy-4 tubes tested in steam with internal heaters. Report NUREG/CR-0343, U.S. Nuclear Regulatory Commission, 1978.

[16] D. A. Powers and R. O. Meyer. Cladding swelling and rupture models for LOCA analysis. Report NUREG-0630, U.S. Nuclear Regulatory Commission, 1980.

[17] E. H. Karb, L. Sepold, P. Hofmann, C. Petersen, G. Schanz, and H. Zimmermann. LWR fuel rod behavior during reactor tests under loss-of-coolant conditions: Results of the FR2 in-pile tests. *J. Nucl. Mater.*, 107:55–77, 1982.

[18] E. H. Karb, M. Prüßmann, L. Sepold, P. Hofmann, and G. Schanz. LWR fuel rod behavior in the FR2 in-pile tests simulating the heatup phase of a LOCA. Report KfK 3346, Kernforschungszentrum Karlsruhe, Germany, 1983.

[19] M. E. Markiewicz and F. J. Erbacher. Experiments on ballooning in pressurized and transiently heated Zircaloy-4 tubes. Report KfK 4343, Kernforschungszentrum Karlsruhe, Germany, 1988.

[20] F. J. Erbacher, H. J. Neitzel, and K. Wiehr. Cladding deformation and emergency core cooling of a pressurized water reactor in a LOCA: Summary description of the REBEKA program. Report KfK 4781, Kernforschungszentrum Karlsruhe, Germany, 1990.

[21] F. J. Erbacher and S. Leistikow. A review of Zircaloy fuel cladding behavior in a loss-of-coolant accident. Report KfK 3973, Kernforschungszentrum Karlsruhe, Germany, 1985.

[22] R. Hill. *The Mathematical Theory of Plasticity*. Oxford University Press, Oxford, UK, 1998.

[23] MATLAB Optimization Toolbox. Manual, The Mathworks, Natick, MA, USA, 2016.

[24] S. Leistikow and G. Schanz. Oxidation kinetics and related phenomena of Zircaloy-4 fuel cladding exposed to high temperature steam and hydrogen-steam mixtures under PWR accident conditions. *Nucl. Engng. Des.*, 103:65–84, 1987.

[25] G. Schanz. Recommendations and supporting information on the choice of zirconium oxidation models in severe accident codes. Report FZKA 6827, Forschungszentrum Karlsruhe, Karlsruhe, Germany, 2003.

[26] H. E. Rosinger. A model to predict the failure of Zircaloy-4 fuel sheathing during postulated LOCA conditions. *J. Nucl. Mater.*, 120:41–54, 1984.

[27] H. E. Rosinger, P. C. Bera, and W. R. Clendening. The steady-state creep of Zircaloy-4 fuel cladding from 940 to 1873 K. Report AECL-6193, Atomic Energy of Canada Limited, Pinawa, MB, Canada, 1978.

[28] B. Burton, A. T. Donaldson, and G. L. Reynolds. Interaction of oxidation and creep in Zircaloy-2. In *Zirconium in the Nuclear Industry: Fourth Conference*, volume ASTM

STP 681, pages 561–585, Philadelphia, USA, 1979. American Society for Testing and Materials.

[29] A. S. Rizkalla, R. A. Holt, and J. J. Jonas. Effect of oxygen on the deformation of Zircaloy-2 at elevated temperatures. In *Zirconium in the Nuclear Industry: Fourth Conference*, volume ASTM STP 681, pages 497–513, Philadelphia, USA, 1979. American Society for Testing and Materials.

[30] R. Choubey, J. J. Jonas, R. A. Holt, and C. E. Ells. Flow stress of oxygen-enriched Zircaloy-2 between 1023 and 1873 K. In D. G. Franklin, editor, *Zirconium in the Nuclear Industry: Fifth Conference*, volume ASTM STP 754, pages 350–369, Philadelphia, USA, 1982. American Society for Testing and Materials.

[31] D. Kaddour, S. Frechinet, A. F. Gourgues, J. C. Brachet, L. Portier, and A. Pineau. Experimental determination of creep properties of zirconium alloys together with phase transformation. *Scripta Mater.*, 51:515–519, 2004.

[32] P. Van Uffelen, C. Győri, A. Schubert, J. van de Laar, Z. Hózer, and G. Spykman. Extending the application range of a fuel performance code from normal operating to design basis accident conditions. *J. Nucl. Mater.*, 383:137–143, 2008.

[33] A. R. Massih. High-temperature creep and superplasticity in zirconium alloys. *J. Nucl. Sci. Techn.*, 50(2):21–34, 2013.

[34] B. Brzoska, G. Cheliotis, A. Kunick, and G. Senski. A new high temperature deformation model for Zircaloy clad ballooning under hypothetical LOCA conditions. In *Fourth International Conference on Structural Mechanics in Reactor Technology (SMiRT-4)*, volume C, Paper C 1/8, San Francisco, CA, USA, August 15-19, 1977.

[35] J. C. Nash. *Nonlinear Parameter Optimization Using R tools*. Wiley, Chichester, UK, 2014.

[36] J. A. Nelder and R. Mead. A simplex method for function minimization. *Computer Journal*, 7(4):308–313, 1965.

[37] European Commission. Fuel cladding failure criteria. Report EUR 19256 EN, European Commission Directorate-General Environment, 2000.

[38] J. Stuckert, M. Grosse, M. Steinbrück, M. Walter, and A. Wensauer. Results of the QUENCH-LOCA experimental program at KIT. *J. Nucl. Mater.*, 534:Paper 152143, 2020.

[39] M. Billone, Y. Yan, T. Burtseva, and R. Daum. Cladding embrittlement during postulated loss-of-coolant accidents. Report NUREG/CR-6967, U.S. Nuclear Regulatory Commission, Washington DC, USA, 2008.

[40] M. C. Billone, Y. Yan, T. A. Burtseva, and R. O. Meyer. Cladding embrittlement during postulated loss-of-coolant accidents. Report NUREG/CR-7219, U.S. Nuclear Regulatory Commission, Washington DC, USA, 2016.

[41] M. E. Flanagan, P. Askeljung, and A. Puranen. Post-test examination results from integral, high-burnup, fueled LOCA tests at Studsvik Nuclear Laboratory. Report NUREG-2160, U.S. Nuclear Regulatory Commission, Washington, DC, USA, 2013.

[42] W. Schilling and H. Ullmaier. Physics of radiation damage in metals. In R. W. Cahn, P. Haasen, and E. J. Kramer, editors, *Material Science and Technology*. Wiley - VCH Verlag GmbH & Co KGaA, Berlin, Germany, 2006.

[43] T. Torimaru, T. Yasuda, and M. Naka. Changes in mechanical properties of irradiated Zircaloy-2 fuel cladding due to short term annealing. *J. Nucl. Mater.*, 238(2-3):169–174, 1996.

[44] J. C. Brachet, L. Portier, and T. Forgeron. Influence of hydrogen content on the α/β phase transformation temperatures and on the thermal-mechanical behavior of Zy-4, M4 (ZrSnFeV), and M5$^{\mathrm{TM}}$ (ZrNbO) alloys during the first phase of LOCA transient. In G. D. Moan and P. Rudling, editors, *Zirconium in the Nuclear Industry: Thirteenth International Symposium*, volume ASTM STP 1423, pages 673–701, West Conshohocken, PA, USA, 2002. American Society for Testing and Materials.

[45] L. Portier, T. Bredel, J-C. Brachet, V. Maillot, J-P. Mardon, and A. Lesbros. Influence of long service exposures on the thermal mechanical behavior of Zy-4 and M5$^{\mathrm{TM}}$ alloys in LOCA conditions. *J. ASTM International*, 2(2):Paper ID JAI12468, 2005.

[46] V. Georgenthum, J. Desquines, and V. Bessiron. Influence of outer zirconia transient cracking and spalling on thermomechanical behaviour of high burnup fuel rod submitted to RIA. *J. Nucl. Sci. Techn.*, 43(9):1089–1096, 2006.

[47] L. O. Jernkvist. Prediction of failure of highly irradiated Zircaloy clad tubes under reactivity initiated accidents. In *Seventeenth International Conference on Structural Mechanics in Reactor Technology (SMiRT-17)*, volume C, pages Paper C03–4, Prague, Czech Republic, August 17-22, 2003.

[48] J. H. Kim, B. K. Choi, J. H. Baek, and Y. H. Jeong. Effects of oxide and hydrogen on the behavior of Zircaloy-4 cladding during the loss of the coolant accident (LOCA). *Nucl. Engng. Des.*, 236:2386–2393, 2006.

[49] A. T. Motta, L. Capolungo, L. Q. Chen, M. Nedim Cinbiz, M. R. Daymond, D. A. Koss, E. Lacroix, G. Pastore, P. C. A. Simon, M. R. Tonks, B. D. Wirth, and M. A. Zikry. Hydrogen in zirconium alloys: A review. *J. Nucl. Mater.*, 518:440–460, 2019.

[50] F. Nagase and T. Fuketa. Effect of pre-hydriding on thermal shock resistance of Zircaloy-4 cladding under simulated loss-of-coolant accident conditions. *J. Nucl. Sci. Techn.*, 41(7):723–730, 2004.

[51] F. Nagase and T. Fuketa. Behavior of pre-hydrided Zircaloy-4 cladding under simulated LOCA conditions. *J. Nucl. Sci. Techn.*, 42(2):209–218, 2005.

[52] R. Thieurmel, J. Besson, E. Pouillier, A. Parrot, A. Ambard, and A. F. Gourgues-Lorenzon. Contribution to the understanding of brittle fracture conditions of zirconium alloy fuel cladding tubes during LOCA transient. *J. Nucl. Mater.*, 527:Paper 151815, 2019.

[53] F. Nagase and T. Fuketa. Fracture behavior of irradiated Zircaloy-4 cladding under simulated LOCA conditions. *J. Nucl. Sci. Techn.*, 43(9):1114–1119, 2006.

[54] F. Nagase, T. Chuto, and T. Fuketa. Behavior of high burn-up fuel cladding under LOCA conditions. *J. Nucl. Sci. Techn.*, 46(7):763–769, 2009.

[55] S. Suman. Influence of hydrogen concentration on burst parameters of Zircaloy-4 cladding tube under simulated loss-of-coolant accident. *Nucl. Engng. and Techn.*, 52(9):2047–2053, 2020.

[56] Y. Yan, T. A. Burtseva, R. O. Meyer, and M. C. Billone. Update of LOCA-integral and post-LOCA-bend test results for fresh ZIRLO cladding. Argonne National Laboratory letter report to U.S. Nuclear Regulatory Commission, July 2010. US NRC ADAMS Accession No. ML111380437.

[57] Y. Yan, T.A. Burtseva, R. O. Meyer, and M. C. Billone. Argonne results for ANL-Studsvik benchmark tests. Argonne National Laboratory letter report to U.S. Nuclear Regulatory Commission, August 2010. US NRC ADAMS Accession No. ML111380445.

[58] M. C. Billone. Assessment of current test methods for post-LOCA cladding behavior. Report NUREG/CR-7139, U.S. Nuclear Regulatory Commission, Washington DC, USA, 2012.

[59] M. E. Flanagan. Mechanical behavior of ballooned and ruptured cladding. Report NUREG-2119, U.S. Nuclear Regulatory Commission, 2012.

A Experimental database

A.1 Definitions

The hoop burst strains presented throughout this report are logarithmic (true) strains, defined in one dimension by

$$\varepsilon = \ln(L/L_o), \tag{A.1}$$

where L is the deformed length of an initial length L_o. Hence, the elongation ΔL is $L - L_o$. From the definition of engineering strain

$$\varepsilon^{eng} = \Delta L/L_o, \tag{A.2}$$

it follows that $\varepsilon = \ln(1 + \varepsilon^{eng})$. This relation has been used for transforming engineering hoop burst strain data in the literature sources to logarithmic hoop burst strains presented in this report.

From the definition of logarithmic strain, it is clear that the average cladding radius and cladding wall thickness in the deformed state are related to the un-deformed geometry and cladding logarithmic hoop strain by

$$R_{av}(t) = R_o \exp(\varepsilon_{\theta\theta}(t)), \tag{A.3}$$

$$W(t) = W_o \exp(\varepsilon_{rr}(t)) = W_o \exp(-\varepsilon_{\theta\theta}(t)). \tag{A.4}$$

Here, R_o and W_o are the initial (un-deformed) values for the cladding average radius and wall thickness. We note that $R_o = (R_{coo} + R_{cio})/2$ and $W_o = R_{coo} - R_{cio}$, where R_{cio} and R_{coo} are the un-deformed inner and outer radii of the cladding tube. The relation $\varepsilon_{rr} = -\varepsilon_{\theta\theta}$ in equation (A.4) results from the simplifying assumption of isotropic creep in the overpressurized cladding tube; see equations (9)-(10) in Section 2.2.

The burst hoop stress presented in this report is not the nominal hoop burst stress reported in many of the literature sources, but rather the Cauchy hoop stress, as defined by equation (6) in section 2.2. This is the stress measure calculated and used by the `FRAPTRAN-QT-1.5` and `ftmat` programs. It is calculated with consideration of the cladding deformation (increase in average radius and decrease in wall thickness). More precisely, by combining equation (6) with equations (A.3)-(A.4), we get

$$\sigma_{\theta\theta}(t) = \Delta P(t) \frac{R_o}{W_o} \exp(2\varepsilon_{\theta\theta}), \tag{A.5}$$

where we recall that $\varepsilon_{\theta\theta}$ is the logarithmic hoop strain. With the engineering strain definition, often used in the literature sources mentioned below, we get

$$\sigma_{\theta\theta}(t) = \Delta P(t) \frac{R_o}{W_o} (1 + \varepsilon_{\theta\theta}^{eng})^2. \tag{A.6}$$

Burst test data from the experimental series considered in this report are presented in the following. The tables have a common format, where the columns contain the following data:

1. Test sample name/identifier/label, ID (-)
2. Initial temperature, T_o (K)
3. Heating rate, $\dot{T}$ (Ks^{-1})
4. Initial overpressure at temperature T_o, ΔP_o (MPa)
5. Maximum overpressure during test, ΔP_m (MPa)
6. Overpressure at time of burst, ΔP_b (MPa)
7. Burst time from start of heating from temperature T_o, t_b (s)
8. Burst temperature, T_b (K)
9. Burst hoop logarithmic strain, ε_b (-)
10. Burst hoop Cauchy stress, σ_b (MPa)
11. Test rod burnup, if pre-irradiated, BU (MWd(kgU)$^{-1}$)

It should be remarked that the literature sources do not always contain all these data. For example, the heating rate may not be explicitly given, but it can be calculated from given data for T_o, T_b and t_b. Similarly, the burst time may not be explicitly given, but it can be calculated from given data for T_o, T_b and $\dot{T}$.

A.2 Data used for model calibration

A.2.1 ORNL-79 test series

The ORNL-79 test series includes 40 out-of-reactor burst tests with transient heating, conducted on fresh (un-irradiated) Zircaloy-4 cladding in steam atmosphere at the Oak Ridge National Laboratory (ORNL), USA [14, 15]. The cladding samples had an outer diameter of 10.92 mm and a wall thickness of 0.635 mm. The samples were not tested in as-fabricated state, but slightly pre-oxidized in superheated steam for 30 minutes at 750 K, resulting in a 1-2 μm thick oxide. The cladding samples were heated internally by use of electrical resistance heaters, and the heated length was 915 mm. The cladding initial temperature was around 615 K in the tests, and the heating rate normally 25-30 Ks^{-1}. The initial internal overpressure in the samples ranged from 0.8 to 20.8 MPa, which is a wider span than in other test series considered in this report

Table A.1: Data from the ORNL-79 burst test series on as-fabricated Zircaloy-4 samples [14–16].

Test ID	T_o [K]	$\dot{T}$ [Ks^{-1}]	ΔP_o [MPa]	ΔP_m [MPa]	ΔP_b [MPa]	t_b [s]	T_b [K]	ε_b [-]	σ_b [MPa]
PS-1	624	27.0	6.35	6.94	6.26	20.0	1166	0.166	70.6
PS-3	607	26.8	6.42	6.76	5.48	20.0	1146	0.255	73.9
PS-4	616	25.0	6.34	6.68	5.76	21.0	1144	0.191	68.3
PS-5	616	25.0	6.31	6.66	5.62	21.5	1155	0.231	72.3
PS-8	622	22.9	6.37	6.71	5.90	21.5	1116	0.182	68.8
PS-9	619	22.5	6.38	6.79	5.55	23.0	1139	0.223	70.2
PS10	625	25.8	6.34	6.73	5.90	21.2	1174	0.182	68.8
PS-12	613	25.6	6.42	6.80	6.04	21.7	1171	0.166	68.1
PS-14	610	24.0	6.35	6.73	5.72	22.6	1156	0.223	72.4
PS-15	625	25.3	6.39	6.68	6.06	20.9	1158	0.157	67.2
PS-17	613	27.1	13.17	13.78	12.03	16.1	1051	0.223	152.2
PS-18	623	19.4	0.70	0.76	0.67	42.0	1444	0.215	8.3
PS-19	621	22.2	2.49	2.72	2.49	27.5	1232	0.247	33.0
SR-1	620	25.8	0.75	0.81	0.70	31.6	1439	0.231	9.0
SR-2	617	28.6	1.03	1.12	0.91	25.7	1355	0.365	15.3
SR-3	619	29.6	1.67	1.80	1.62	22.4	1284	0.358	26.8
SR-4	610	28.2	4.30	4.60	4.38	20.6	1194	0.157	48.6
SR-5	618	25.7	10.02	10.38	9.42	18.0	1083	0.231	121.1
SR-7	611	25.5	15.01	15.43	14.34	15.5	1009	0.182	167.2
SR-8	609	27.1	1.32	1.42	1.13	25.1	1293	0.358	18.7
SR-13	598	30.5	1.21	1.33	0.97	24.6	1352	0.582	25.2
SR-15	615	25.6	20.25	21.18	19.05	14.5	987	0.131	200.5
SR-17	617	27.8	1.21	1.31	0.96	25.2	1322	0.425	18.2
SR-19	608	24.1	19.87	20.73	18.94	14.6	961	0.148	206.4
SR-20	605	28.5	1.19	1.31	0.96	25.1	1322	0.438	18.7
SR-21	613	27.8	1.21	1.33	1.02	24.5	1296	0.392	18.1
SR-22	605	27.4	1.03	1.13	0.79	27.2	1354	0.405	14.4
SR-23	609	28.7	1.02	1.13	0.86	25.7	1350	0.300	12.7
SR-24	605	26.9	1.10	1.20	0.89	26.9	1330	0.513	20.1
SR-25	618	28.1	1.03	1.14	0.86	26.5	1365	0.577	22.1
SR-26	613	26.3	0.90	0.96	0.73	29.9	1403	0.293	10.6
SR-27	613	27.6	1.03	1.09	0.82	26.9	1357	0.344	13.2
SR-28	608	25.8	8.83	9.30	8.30	19.3	1108	0.239	108.4
SR-29	613	25.0	8.58	8.95	7.94	20.0	1116	0.239	103.7
SR-37	578	26.0	14.31	14.86	13.46	17.4	1033	0.207	164.9
SR-38	613	27.6	14.56	15.16	13.67	15.5	1043	0.182	159.4
SR-41	613	8.8	10.41	10.81	9.66	46.9	1030	0.239	126.2
SR-42	617	8.8	10.39	10.80	9.36	47.1	1034	0.247	124.2
SR-43	613	4.8	8.36	8.70	7.52	89.1	1046	0.255	101.3
SR-44	655	4.7	7.83	8.15	7.21	82.5	1050	0.262	98.7

A.2.2 KfK-83(F) test series

The KfK-83(F) test series includes 19 in-reactor burst tests conducted on fresh (F) test fuel rods with Zircaloy-4 cladding in the FR2 research reactor, Germany [17, 18]. Most of the test rods were charged with UO_2 fuel pellets and heated by nuclear fission reactions, but 7 rods were fuel rod simulators (Brennstabsimulator - BSS) with internal electrical heaters. The heated length was around 500 mm for all test rods, both UO_2-charged and electrically heated. The cladding tube dimensions were identical for all rods: they had an outer diameter of 10.75 mm and a wall thickness of 0.725 mm. The exact initial cladding temperature for individual tests is not reported. Based on the data presented for selected tests, the initial temperature has been assumed to be 600 K for all tests. The heating rates given below are calculated from this assumption and the burst times and burst temperatures reported for each test.

Table A.2: Data from the KfK-83 burst test series on fresh (un-irradiated) Zircaloy-4 samples [17, 18]. Test rods BSS12-BSS28 were electrically heated.

Test ID	T_o [K]	$\dot{T}$ [Ks^{-1}]	ΔP_o [MPa]	ΔP_m [MPa]	ΔP_b [MPa]	t_b [s]	T_b [K]	ε_b [-]	σ_b [MPa]
A1.1	600	6.0	5.10	5.30	4.90	79.0	1083	0.495	91.1
A2.1	600	24.5	9.30	9.90	8.70	20.0	1093	0.307	111.3
A2.2	600	13.9	6.60	7.40	5.70	38.0	1133	0.445	95.9
A2.3	600	12.4	2.50	2.60	2.40	55.0	1288	0.300	30.2
B1.1	600	14.2	5.50	5.80	5.10	40.0	1173	0.255	58.7
B1.2	600	8.1	4.90	5.40	4.40	72.0	1188	0.231	48.3
B1.3	600	13.9	6.50	7.00	6.00	37.0	1118	0.293	74.5
B1.5	600	8.0	5.10	5.70	4.40	72.0	1183	0.470	77.9
B1.6	600	8.8	8.40	8.90	7.90	56.0	1098	0.322	104.0
B1.7	600	12.4	6.50	7.00	6.00	41.0	1113	0.293	74.5
B3.1	600	10.7	8.40	9.00	7.80	46.0	1098	0.315	101.2
B3.2	600	10.6	5.50	6.00	4.90	55.0	1188	0.405	76.2
BSS12	600	10.9	6.20	7.10	5.30	47.0	1115	0.300	66.8
BSS22	600	9.8	5.00	5.80	4.10	54.0	1135	0.495	76.2
BSS23	600	13.1	8.70	9.40	8.00	37.0	1088	0.336	108.4
BSS24	600	12.3	2.50	2.50	2.40	51.0	1231	0.262	28.0
BSS25	600	13.5	11.20	11.90	10.50	31.0	1020	0.255	120.8
BSS26	600	13.7	9.80	10.80	8.80	34.0	1068	0.351	122.7
BSS28	600	10.4	2.00	2.10	1.90	61.0	1240	0.293	23.6

A.2.3 KfK-83(I) test series

The KfK-83(I) test series includes 22 in-reactor burst tests conducted on irradiated (I) test fuel rods with Zircaloy-4 cladding in the FR2 research reactor, Germany [17, 18]. All test rods were charged with UO_2 fuel pellets and had been pre-irradiated to burnups from 2.5 to 35 MWd(kgU)$^{-1}$ in the FR2; see Table A.3. The fuel rod and cladding dimensions were the same as in the KfK-83(F) test series; see Section A.2.2. The exact initial cladding temperature for individual tests is not reported. Based on the data presented for selected tests, the initial temperature has been assumed to be 600 K for all tests. The heating rates given below are calculated from this assumption and the burst times and burst temperatures reported for each test.

Table A.3: Data from the KfK-83 burst test series on pre-irradiated Zircaloy-4 samples [17, 18].

Test ID	T_o [K]	$\dot{T}$ [Ks^{-1}]	ΔP_o [MPa]	ΔP_m [MPa]	ΔP_b [MPa]	t_b [s]	T_b [K]	ε_b [-]	σ_b [MPa]	BU [MWd]
C1	600	12.1	5.00	5.50	4.50	47.0	1173	0.412	70.9	2.5
C2	600	10.6	3.10	3.30	2.90	58.0	1218	0.329	38.7	2.5
C3	600	13.1	10.40	11.10	9.70	32.0	1022	0.315	125.9	2.5
C4	600	11.8	7.20	8.00	6.40	41.0	1088	0.365	91.8	2.5
C5	600	7.5	2.30	2.40	2.10	78.0	1189	0.482	38.1	2.5
E1	600	9.8	2.40	2.50	2.20	59.0	1183	0.262	25.7	8.0
E2	600	13.0	12.00	12.80	11.20	29.0	981	0.378	165.1	8.0
E3	600	11.2	5.20	5.50	4.80	47.0	1133	0.270	57.0	8.0
E4	600	12.9	7.80	8.50	7.10	35.0	1054	0.438	117.9	8.0
E5	600	8.3	2.20	2.50	1.80	63.0	1129	0.513	34.7	8.0
F1	600	13.0	6.30	7.10	5.50	43.0	1163	0.464	96.1	20.0
F2	600	9.8	5.70	6.10	5.20	57.0	1166	0.322	68.5	20.0
F3	600	10.5	4.30	4.50	4.10	57.0	1205	0.239	45.7	20.0
F4	600	13.6	7.70	8.30	7.10	37.0	1108	0.293	88.1	20.0
F5	600	11.2	6.50	7.10	5.90	49.0	1153	0.344	81.1	20.0
G1.2	600	7.2	7.10	7.40	6.70	55.0	1003	0.262	78.3	35.0
G1.3	600	7.9	4.50	5.00	4.00	70.0	1163	0.482	72.6	35.0
G1.4	600	7.8	8.60	9.00	8.20	58.0	1058	0.285	100.3	35.0
G1.5	600	7.5	5.50	5.90	5.10	60.0	1053	0.344	70.1	35.0
G2.2	600	16.6	7.00	7.40	6.50	31.0	1119	0.247	73.6	35.0
G3.2	600	15.4	6.40	7.30	5.60	33.0	1111	0.344	77.0	35.0
G3.3	600	14.5	11.90	12.70	11.00	29.0	1023	0.278	132.5	35.0

A.2.4 KfK-88(C) test series

The KfK-88(C) test series includes 23 out-of-reactor burst tests with transient heating, conducted on fresh Zircaloy-4 cladding in steam atmosphere in the REBEKA test facility, Kernforschungszentrum Karlsruhe, Germany [19, 20]. The material in these tests was PHWR Zircaloy-4 cladding manufactured by CONVAR in Argentina. The main purpose of the tests was to compare the behaviour of this material with that produced by NRG in Germany; see the KfK-88(N) tests in Section A.2.5 below. As-fabricated cladding samples were heated from inside by use of electrical resistance heaters with a heated length of 325 mm. In addition, the samples were heated from outside by a shroud electrical heater. This created a near-uniform temperature distribution in the samples. The heating was slow, to simulate the expected LOCA conditions in a PHWR. All samples had a nominal outer diameter of 11.90 mm and a wall thickness of 0.550 mm.

Table A.4: Data from the KfK-88(C) burst test series on Zircaloy-4 CONVAR samples [19, 20].

Test ID	T_o [K]	$\dot{T}$ [Ks^{-1}]	ΔP_o [MPa]	ΔP_m [MPa]	ΔP_b [MPa]	t_b [s]	T_b [K]	ε_b [-]	σ_b [MPa]
1	619	1.0	3.90	3.90	3.90	450.0	1105	0.610	136.2
2	616	1.0	3.90	3.90	3.90	442.0	1093	0.531	116.3
3	625	1.0	3.90	3.90	3.90	450.0	1111	0.723	170.8
4	618	1.0	5.30	5.30	5.30	399.0	1049	0.688	216.6
5	611	1.0	5.30	5.30	5.30	398.0	1041	0.565	169.4
6	621	1.0	5.30	5.30	5.30	407.0	1061	0.560	167.5
7	625	1.0	6.60	6.60	6.60	376.0	1031	0.728	291.8
8	624	1.0	6.60	6.60	6.60	382.0	1037	0.615	233.1
10	621	1.0	7.90	7.90	7.90	348.0	997	0.554	246.8
11	613	1.0	7.90	7.90	7.90	358.0	1000	0.542	241.1
12	618	1.0	7.90	7.90	7.90	351.0	997	0.565	252.5
13	619	1.0	9.30	9.30	9.30	337.0	983	0.531	277.3
14	622	1.0	9.30	9.30	9.30	339.0	988	0.577	304.0
15	614	1.0	9.30	9.30	9.30	341.0	982	0.513	267.6
17	626	1.0	2.60	2.60	2.60	496.0	1162	0.438	64.5
18	625	1.0	2.60	2.60	2.60	497.0	1162	0.419	62.0
27	620	1.0	9.70	9.70	9.70	330.0	976	0.554	303.0
28	619	1.0	4.60	4.60	4.60	415.0	1067	0.703	193.7
29	618	1.0	2.20	2.20	2.20	515.0	1174	0.372	47.7
39	642	1.0	1.24	1.24	1.24	545.0	1231	0.519	36.1
40	634	1.0	1.24	1.24	1.24	555.0	1233	0.445	31.1
41	628	1.0	0.55	0.55	0.55	608.0	1285	0.231	9.0
42	629	1.0	0.55	0.55	0.55	604.0	1281	0.215	8.7

A.2.5 KfK-88(N) test series

The KfK-88(N) test series includes 18 out-of-reactor burst tests with transient heating, conducted on fresh Zircaloy-4 cladding in steam atmosphere in the REBEKA test facility, Kernforschungszentrum Karlsruhe, Germany [19, 20]. The tested material was PHWR Zircaloy-4 cladding manufactured by NRG in Germany. The dimensions of the cladding samples and the testing conditions were identical to those in the KfK-88(C) test series; see Section A.2.4 above.

Table A.5: Data from the KfK-88(N) burst test series on Zircaloy-4 NRG samples [19, 20].

Test ID	T_o [K]	$\dot{T}$ [Ks^{-1}]	ΔP_o [MPa]	ΔP_m [MPa]	ΔP_b [MPa]	t_b [s]	T_b [K]	ε_b [-]	σ_b [MPa]
1	630	1.0	3.90	3.90	3.90	420.0	1084	0.548	120.4
2	622	1.0	3.90	3.90	3.90	416.0	1071	0.599	133.3
3	624	1.0	3.90	3.90	3.90	431.0	1089	0.631	142.2
4	618	1.0	5.30	5.30	5.30	401.0	1051	0.658	203.7
6	609	1.0	5.30	5.30	5.30	404.0	1045	0.525	156.2
7	618	1.0	6.30	6.30	6.30	366.0	1013	0.513	181.3
8	626	1.0	6.60	6.60	6.60	372.0	1028	0.542	201.5
9	610	1.0	6.60	6.60	6.60	377.0	1017	0.565	210.9
10	607	1.0	6.60	6.60	6.60	370.0	1007	0.571	213.4
11	622	1.0	7.90	7.90	7.90	354.0	1004	0.582	261.2
12	624	1.0	7.90	7.90	7.90	348.0	1000	0.565	252.5
13	637	1.0	7.90	7.90	7.90	336.0	1000	0.637	291.2
14	621	1.0	9.30	9.30	9.30	332.0	980	0.571	300.6
15	622	1.0	9.30	9.30	9.30	333.0	982	0.621	332.0
16	618	1.0	9.30	9.30	9.30	336.0	981	0.542	283.9
17	621	1.0	2.60	2.60	2.60	490.0	1150	0.470	68.7
18	618	1.0	2.60	2.60	2.60	502.0	1160	0.489	71.3
19	622	1.0	2.60	2.60	2.60	500.0	1162	0.470	68.7

A.2.6 BARC-17 test series

The BARC-17 test series includes 29 out-of-reactor burst tests with transient heating, conducted on as-fabricated Zircaloy-4 PHWR cladding in steam atmosphere at the Bhabha Atomic Research Centre (BARC), Mumbai, India [13]. The cladding samples had an outer diameter of 15.20 mm and a wall thickness of 0.440 mm, which makes them different from samples in other test series considered in this report. Another difference is that direct electrical heating was used in the tests. From graphs of recorded heating histories in [13], it seems that this heating method resulted in significant temperature gradients in the samples, both axially and circumferentially.

Table A.6: Data from the BARC-17 burst test series on Zircaloy-4 PHWR cladding samples [13].

Test ID	T_o [K]	$\dot{T}$ [Ks^{-1}]	ΔP_o [MPa]	ΔP_m [MPa]	ΔP_b [MPa]	t_b [s]	T_b [K]	ε_b [-]	σ_b [MPa]
3B	516	11.0	0.30	0.47	0.45	77.0	1363	0.177	11.9
3C	427	15.0	0.30	0.34	0.31	63.0	1372	0.085	6.8
5A	410	13.0	0.53	0.59	0.37	73.0	1359	0.148	9.2
5B	351	12.0	0.50	0.57	0.47	82.0	1335	0.222	13.6
5C	397	19.0	0.51	0.60	0.56	45.0	1252	0.269	17.8
8A	449	14.0	0.79	0.84	0.82	54.0	1205	0.263	25.7
8B	391	14.0	0.81	0.88	0.84	55.0	1161	0.208	23.5
8C	547	6.0	0.83	0.98	0.88	98.0	1135	0.270	27.9
10A	408	14.0	1.02	1.17	1.04	54.0	1164	0.254	32.0
10B	382	11.0	1.03	1.15	1.07	73.0	1185	0.200	29.5
10C	591	5.0	1.08	1.17	1.09	115.0	1166	0.208	30.6
20A	430	9.0	2.03	2.22	1.89	79.0	1141	0.142	46.5
20B	407	8.0	1.99	2.22	1.81	92.0	1143	0.324	64.0
20C	471	14.0	2.03	2.16	2.10	45.0	1101	0.188	56.6
30A	360	15.0	2.98	3.32	2.82	51.0	1125	0.279	91.2
30B	369	16.0	3.16	3.40	3.04	44.0	1073	0.252	93.2
30C	580	7.0	3.16	3.55	3.11	71.0	1077	0.369	120.3
40A	354	11.0	4.22	4.56	3.38	63.0	1047	0.508	172.7
40B	430	11.0	4.17	4.69	4.30	53.0	1013	0.517	223.7
40C	544	10.0	4.18	4.87	4.54	47.0	1014	0.317	158.3
50A	382	14.0	5.01	5.50	4.84	43.0	984	0.356	182.3
50B	328	14.0	5.07	5.48	4.74	51.0	1042	0.487	232.1
50C	427	14.0	5.04	5.40	5.03	38.0	959	0.473	239.4
60A	373	18.0	6.13	6.51	6.00	30.0	913	0.237	178.2
60B	380	17.0	6.04	6.56	6.20	31.0	907	0.287	203.8
60C	411	17.0	6.20	6.51	6.15	30.0	921	0.279	198.8
70A	389	15.0	7.16	7.62	7.31	34.0	899	0.215	207.9
70B	378	17.0	7.02	7.24	6.88	29.0	871	0.208	192.9
70C	358	18.0	7.10	7.66	7.08	31.0	916	0.279	228.9

A.3 Data used for independent verification

A.3.1 ANL-08 test series

The ANL-08 test series includes 7 out-of-reactor burst tests on Zircaloy-2 (Zr-1.5Sn-0.2Fe-0.1Cr-0.05Ni by wt%) cladding material, carried out in steam at the Argonne National Laboratory (ANL), USA [39]. The material was commercial cladding material with internal zirconium liner, used for 9×9-type BWR fuel. The cladding outer diameter was 11.18 mm and the wall thickness 0.71 mm. Four tests were done on fresh (as-fabricated) cladding material, whereas three tests were done on samples taken from discharged fuel rods with an average burnup of 56-57 MWd(kgU)$^{-1}$. These samples were moderately corroded, with an external oxide layer of about 10 μm and a hydrogen concentration around 70 wppm [39]. All tests were done under identical conditions to allow comparisons between the samples: they were brought to an initial temperature of 573 K, pressurized to 8.28 MPa and then heated to burst with a constant heating rate of 5 Ks^{-1}. The internal pressure varied moderately during the test, due to gradually increasing sample temperature and internal volume. External heating was used.

Table A.7: Data from the ANL-08 burst test series on fresh (F) and pre-irradiated Zircaloy-2 samples [39].

Test ID	T_o [K]	$\dot{T}$ [Ks^{-1}]	ΔP_o [MPa]	ΔP_m [MPa]	ΔP_b [MPa]	t_b [s]	T_b [K]	ε_b [-]	σ_b [MPa]	BU [MWd]
OCL11	573	5.0	8.28	8.61	7.93	90.6	1026	0.358	119.6	F
OCL13	573	5.0	8.28	9.09	6.43	93.2	1039	0.358	96.9	F
OCL17	573	5.0	8.28	9.10	9.07	90.0	1023	0.399	148.5	F
OCL22	573	5.0	8.28	8.87	6.90	89.4	1020	0.432	120.7	F
ICL2	573	5.0	8.28	8.87	8.01	90.0	1023	0.329	114.1	56.0
ICL3	573	5.0	8.28	9.00	8.60	86.0	1003	0.358	129.7	56.0
ICL4	573	5.0	8.28	8.86	8.00	98.0	1063	0.307	109.1	56.0

A.3.2 ANL-10 test series

The ANL-10 test series includes 22 out-of-reactor burst tests on fresh ZIRLO cladding material of the first generation (Zr-1.0Sn-1.0Nb-0.1Fe by wt%), carried out in steam at ANL. The tests are partially described in many sources [40, 56–59], and the reported results are not always consistent from one source to another. The results presented here are taken from the last, and hopefully the most correct, report [40]. The tested material was ZIRLO cladding of 17×17-type PWR fuel rod design, with an outer diameter of 9.50 mm and a wall thickness of 0.571 mm. The testing conditions were very similar to those used previously by ANL, as described in Section A.3.1 above. The most notable difference is the sample initial pressure, which ranged from 2.8 to 11.0 MPa at 573 K.

Table A.8: Data from the ANL-10 burst test series on as-fabricated ZIRLO cladding samples [40].

Test ID	T_o [K]	$\dot{T}$ [Ks^{-1}]	ΔP_o [MPa]	ΔP_m [MPa]	ΔP_b [MPa]	t_b [s]	T_b [K]	ε_b [-]	σ_b [MPa]
6	573	5.0	8.27	8.55	8.07	90.0	1023	0.351	127.2
7	573	5.0	5.52	5.72	5.45	102.0	1083	0.199	63.4
8	573	5.0	4.14	4.34	4.10	109.0	1118	0.199	47.7
9	573	5.0	2.76	2.93	2.76	115.0	1148	0.285	38.2
10	573	5.0	11.03	11.38	10.27	83.0	988	0.531	232.1
11	573	5.0	9.65	10.00	9.07	90.0	1023	0.336	139.0
12	573	5.0	6.89	7.17	6.62	101.0	1078	0.285	91.6
13	573	5.0	8.27	8.58	8.14	88.2	1014	0.351	128.3
14	573	5.0	8.27	8.48	8.07	87.0	1008	0.392	138.2
15	573	5.0	8.27	8.41	7.79	91.0	1028	0.419	140.7
16	573	5.0	8.27	8.45	7.93	86.8	1007	0.300	113.0
17	573	5.0	8.27	8.48	7.93	90.0	1023	0.372	130.4
18	573	5.0	8.27	8.83	8.76	89.6	1021	0.358	140.1
19	573	5.0	4.14	4.27	4.07	108.0	1113	0.223	49.7
21	573	5.0	4.14	4.34	4.07	110.0	1123	0.247	52.1
22	573	5.0	4.14	4.27	4.14	107.4	1110	0.207	49.0
25	573	5.0	8.27	8.55	7.93	91.4	1030	0.351	125.0
29	573	5.0	8.27	8.55	7.86	89.2	1019	0.399	136.4
32	573	5.0	8.27	8.55	7.79	89.6	1021	0.399	135.2
36	573	5.0	8.27	8.45	7.58	90.0	1023	0.425	138.7
37	573	5.0	8.27	8.48	7.93	91.0	1028	0.378	132.2
43	573	5.0	8.27	8.48	8.00	87.6	1011	0.405	140.7

A.3.3 Studsvik-13 test series

The Studsvik-13 test series includes 6 out-of-reactor burst tests on irradiated ZIRLO cladding material of the first generation, carried out in steam at Studsvik Nuclear, Sweden [41]. The material was sampled from 17×17-type PWR fuel rods, which had been irradiated to rod average burnups of 55 and 68 MWd(kgU)$^{-1}$. The local burnups for the short-length ($\approx$ 300 mm) samples were estimated to 60 and 78 MWd(kgU)$^{-1}$. The cladding outer diameter was 9.50 mm and the wall thickness 0.571 mm. The cladding samples had an external oxide layer of 20-30 μm and hydrogen concentrations of 150-290 wppm [41]. The testing conditions were very similar to those used by ANL, as described above in Sections A.3.1-A.3.2: the sample initial pressure in the Studsvik tests was either 8.2 or 11.0 MPa at 573 K.

Table A.9: Data from the Studsvik-13 burst test series on pre-irradiated ZIRLO samples [41].

Test ID	T_o [K]	$\dot{T}$ [Ks^{-1}]	ΔP_o [MPa]	ΔP_m [MPa]	ΔP_b [MPa]	t_b [s]	T_b [K]	ε_b [-]	σ_b [MPa]	BU [MWd]
189	573	5.0	11.00	11.60	10.90	81.0	973	0.392	186.7	78.0
191	573	5.0	11.00	11.20	10.40	76.0	953	0.405	183.0	78.0
192	573	5.0	8.20	8.40	8.10	81.0	973	0.445	154.1	78.0
193	573	5.0	8.20	8.60	8.10	85.6	1001	0.405	142.5	78.0
196	573	5.0	8.20	8.50	8.10	77.2	959	0.223	99.0	60.0
198	573	5.0	8.20	8.40	8.10	78.6	966	0.223	99.0	60.0

B Model-data comparisons

This appendix contains six series of plots. In each series, the relative differences (D_r) between calculated and measured time to cladding burst and cladding hoop stress at burst are presented for each of the 151 tests in the considered database. The relative differences are plotted as functions of six selected parameters, with the aim to identify trends with regard to these parameters. Results are plotted only for the optimized set of models; see Section 3.1. Uncertainty bands, corresponding to $\pm 1\sigma$ differences between calculated and measured results, are included in all figures; see Table 5.

In summary, the following general conclusions can be drawn from the model-data comparisons in this appendix:

- Some test series reveal trends with regard to specific parameters, such as temperature or heating rate. An example is the BARC-17 test series, where the relative differences between calculated and measured time to burst seem to decrease with increasing burst temperature; see Figure B.3. The trend is clear at least at low temperature ($<$1000 K). However, when *all* test series are considered, or a wider parameter range is assessed, it is difficult to discern any clear trends in the model-data comparisons. In conclusion, one should be careful not to rely on results from a single test series for model calibration, nor should the models be applied to conditions not covered by the database used for calibration.
- The calculated time to burst is within ± 10 % of the measured value for most tests in the database. Outliers, for which the burst time is overestimated by more than 10 %, belong almost exclusively to the BARC-17 and KfK-83(I) test series. For the former, the outliers are characterized by very low burst temperature ($<$930 K). For the latter, effects of sample pre-irradiation on the cladding creep deformation may be responsible for the model-data differences. Figures B.3 and B.9 suggest that the cladding creep at low temperature or low β-phase content for the pre-irradiated samples is faster than calculated by the models.
- The KfK-88 test were done with slow heating (1.1 Ks^{-1}), which resulted in much longer time to cladding burst than for other test series in the database; see Figures B.1-B.2 and B.5- B.6. Notwithstanding the slow heating, the burst times and burst hoop stresses for these tests are reproduced with fair accuracy by the models: the burst times are only slightly underestimated, while the deviations for the burst stresses are somewhat larger. These deviations are linked to the underestimated burst strains for the KfK-88 tests; see Figure 9.

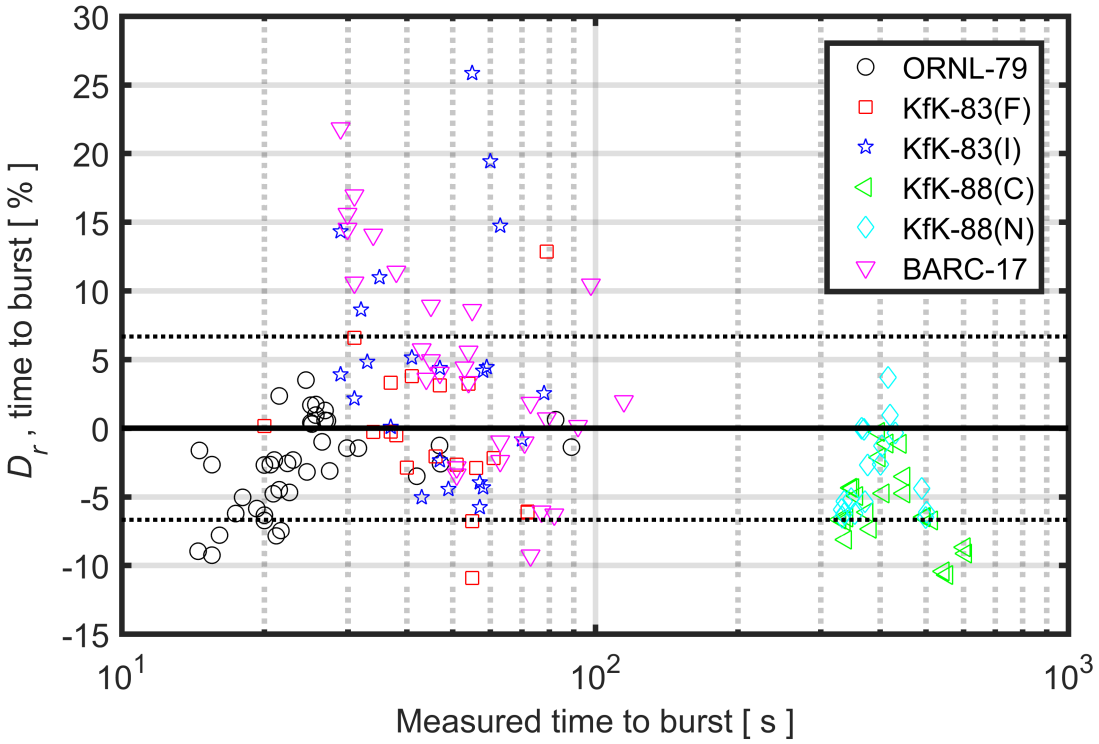

Figure B.1: Relative differences between calculated and measured time to cladding burst, plotted with regard to the measured time to burst for each of the 151 tests.

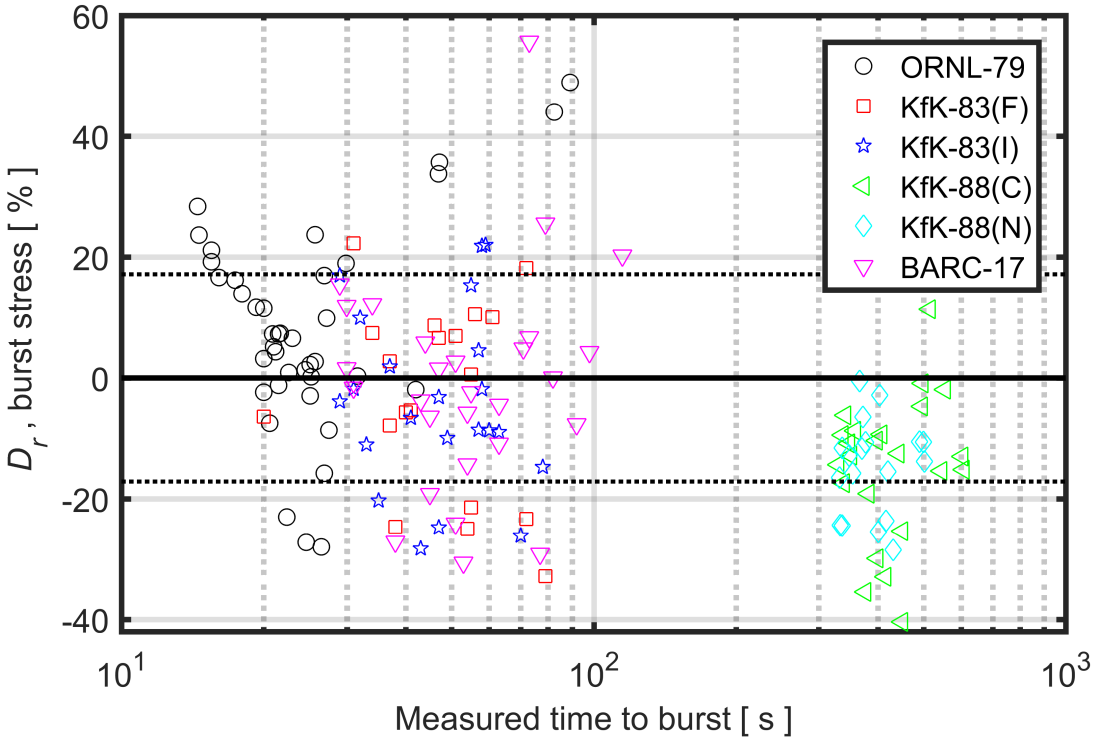

Figure B.2: Relative differences between calculated and measured burst hoop stress, plotted with regard to the measured time to burst for each of the 151 tests.

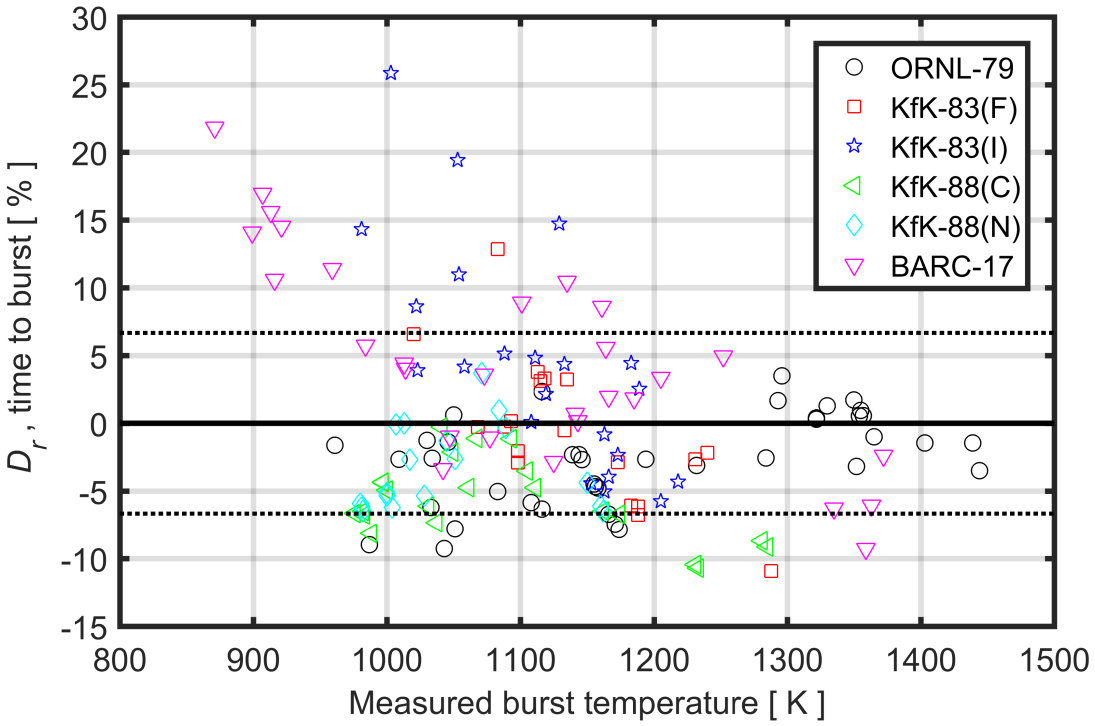

Figure B.3: Relative differences between calculated and measured time to cladding burst, plotted with regard to the measured burst temperature for each of the 151 tests.

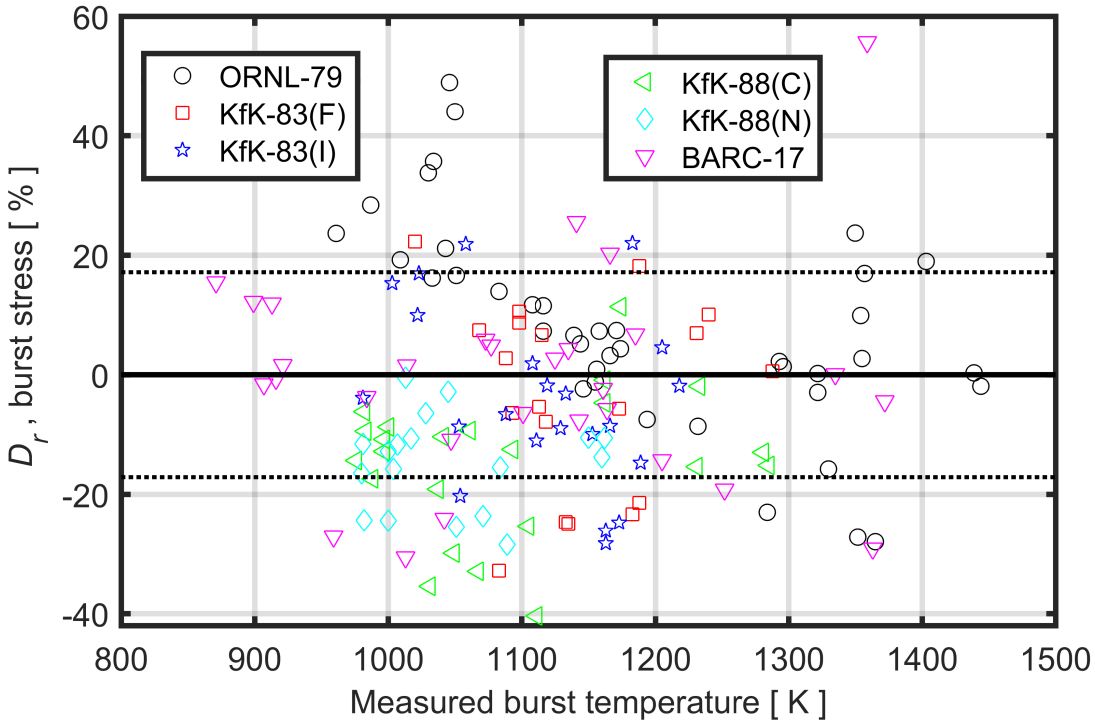

Figure B.4: Relative differences between calculated and measured burst hoop stress, plotted with regard to the measured burst temperature for each of the 151 tests.

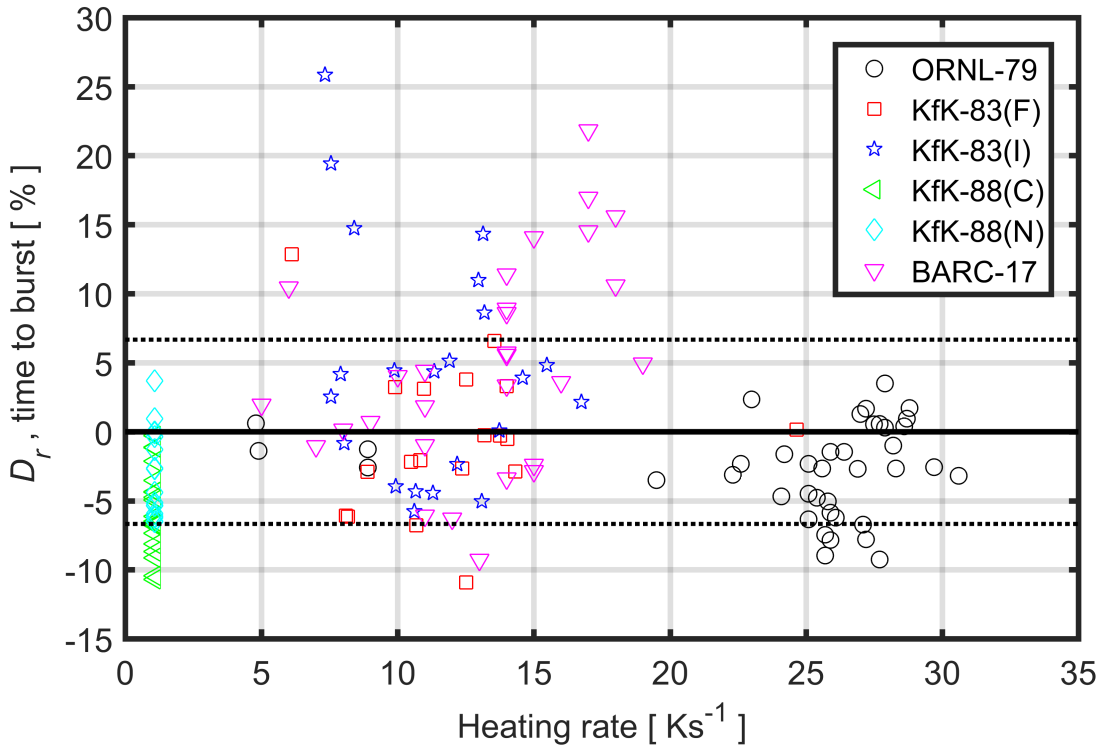

Figure B.5: Relative differences between calculated and measured time to cladding burst, plotted with regard to the heating rate for each of the 151 test samples.

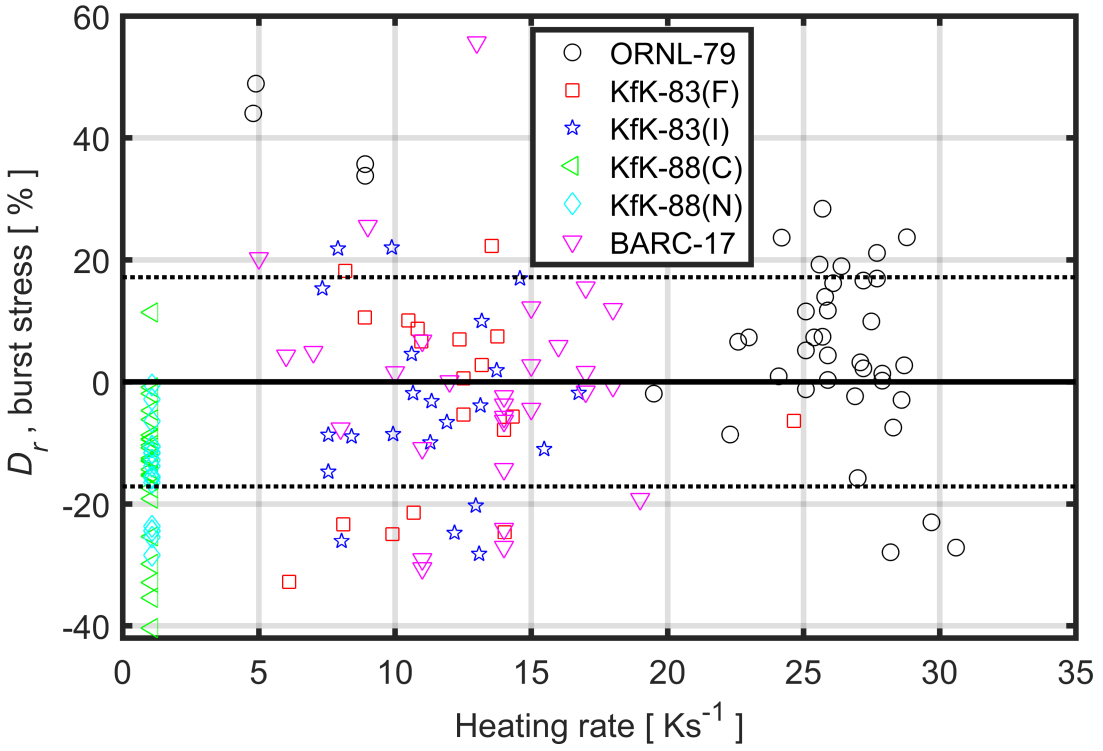

Figure B.6: Relative differences between calculated and measured burst hoop stress, plotted with regard to the heating rate for each of the 151 test samples.

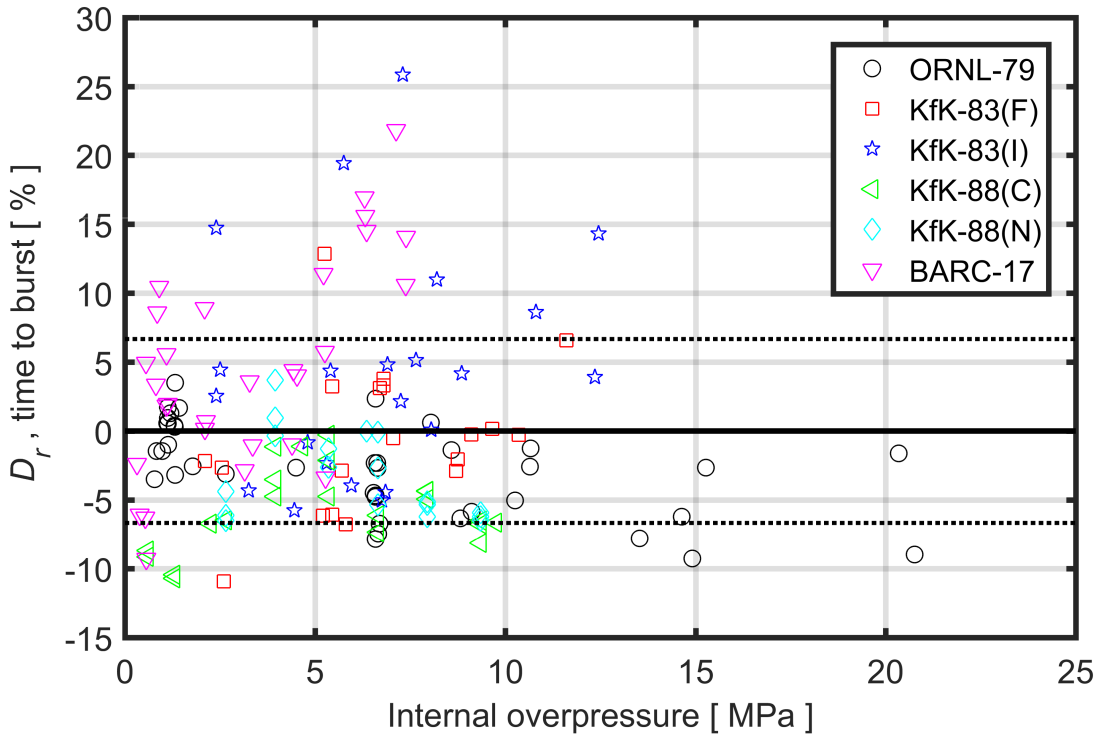

Figure B.7: Relative differences between calculated and measured time to cladding burst, plotted with regard to the internal overpressure (average of ΔP_o and ΔP_m) for each of the 151 test samples.

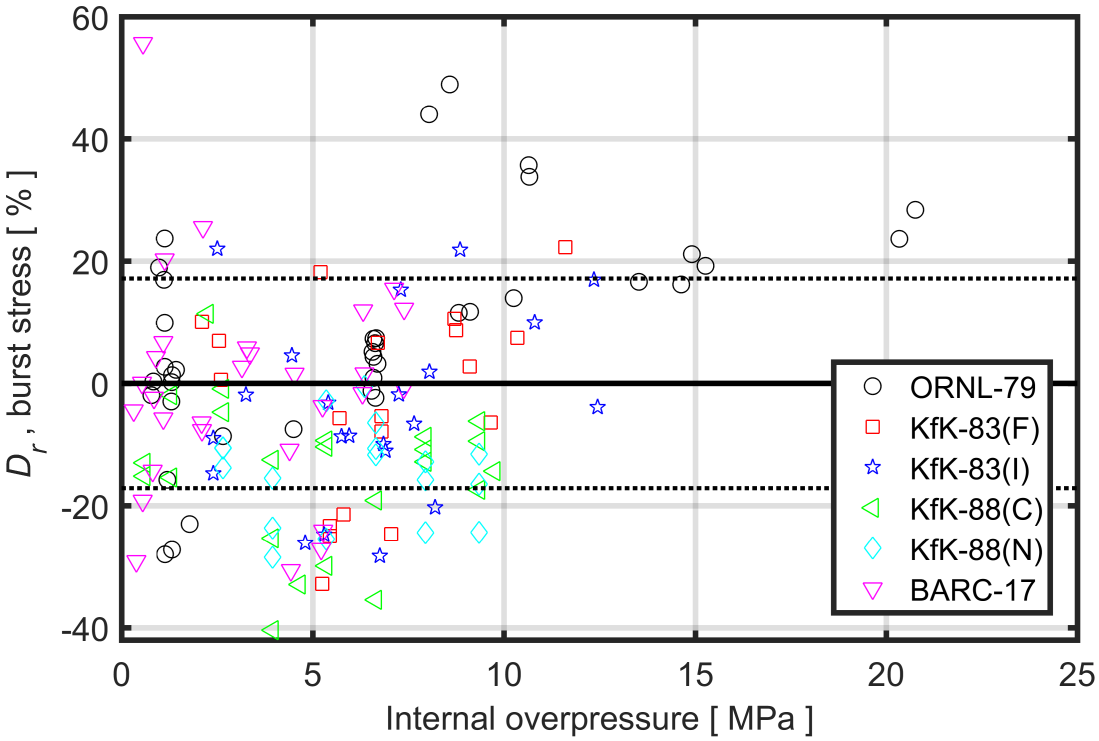

Figure B.8: Relative differences between calculated and measured burst hoop stress, plotted with regard to the internal overpressure (average of ΔP_o and ΔP_m) for each of the 151 test samples.

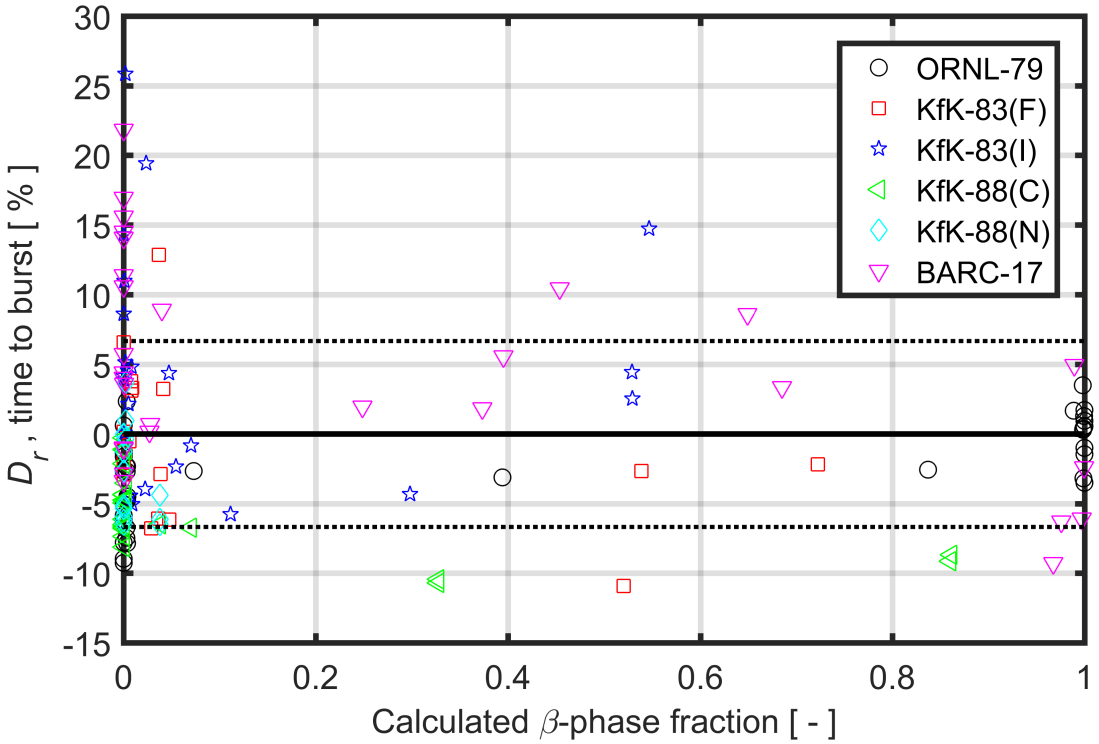

Figure B.9: Relative differences between calculated and measured time to cladding burst, plotted with regard to the calculated β-phase fraction at time of burst for each of the 151 test samples.

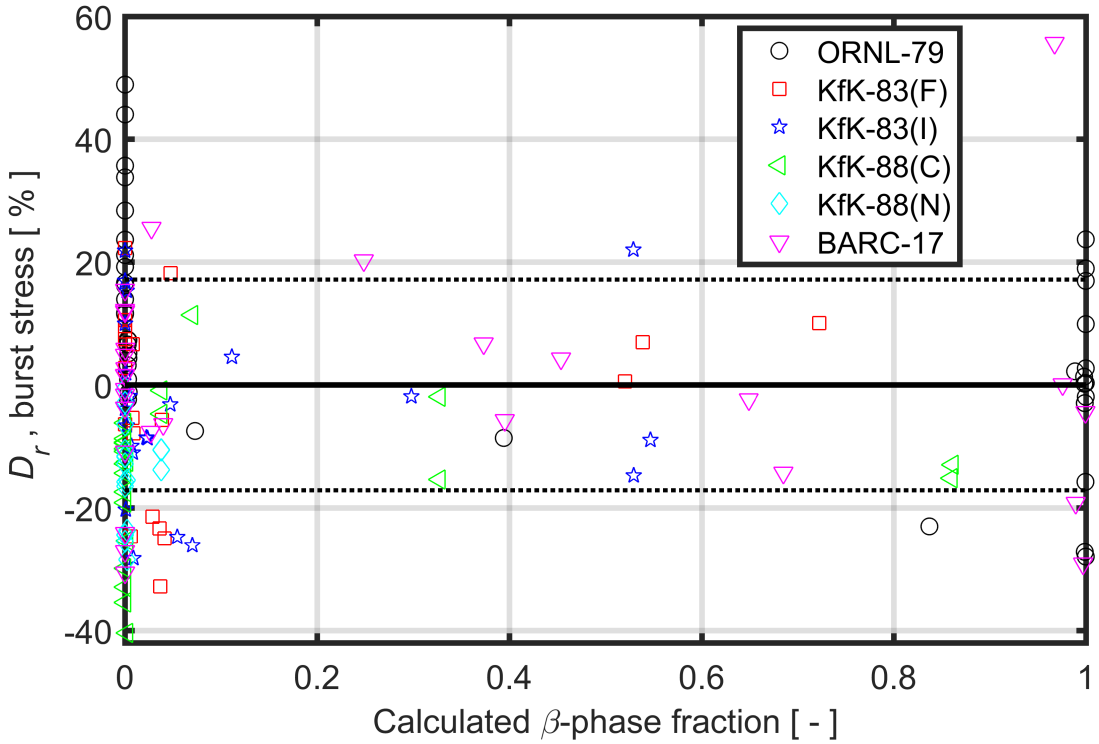

Figure B.10: Relative differences between calculated and measured burst hoop stress, plotted with regard to the calculated β-phase fraction at time of burst for each of the 151 test samples.

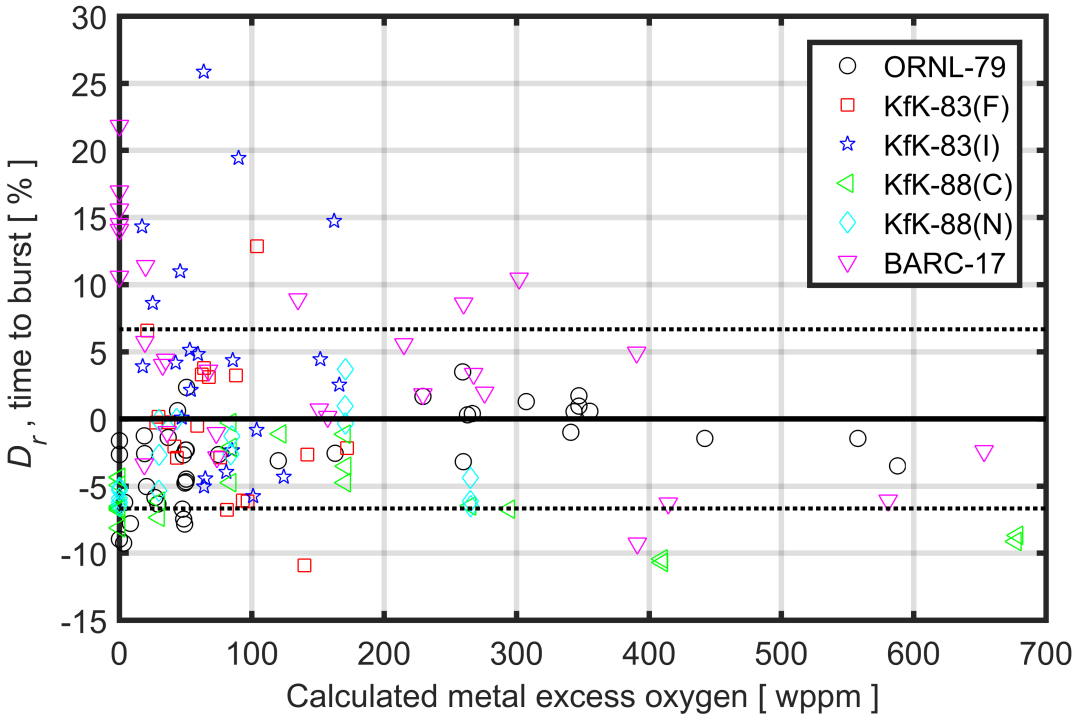

Figure B.11: Relative differences between calculated and measured time to cladding burst, plotted with regard to the calculated concentration of excess oxygen in the cladding metal (x_{Met}) at time of burst for each of the 151 test samples.

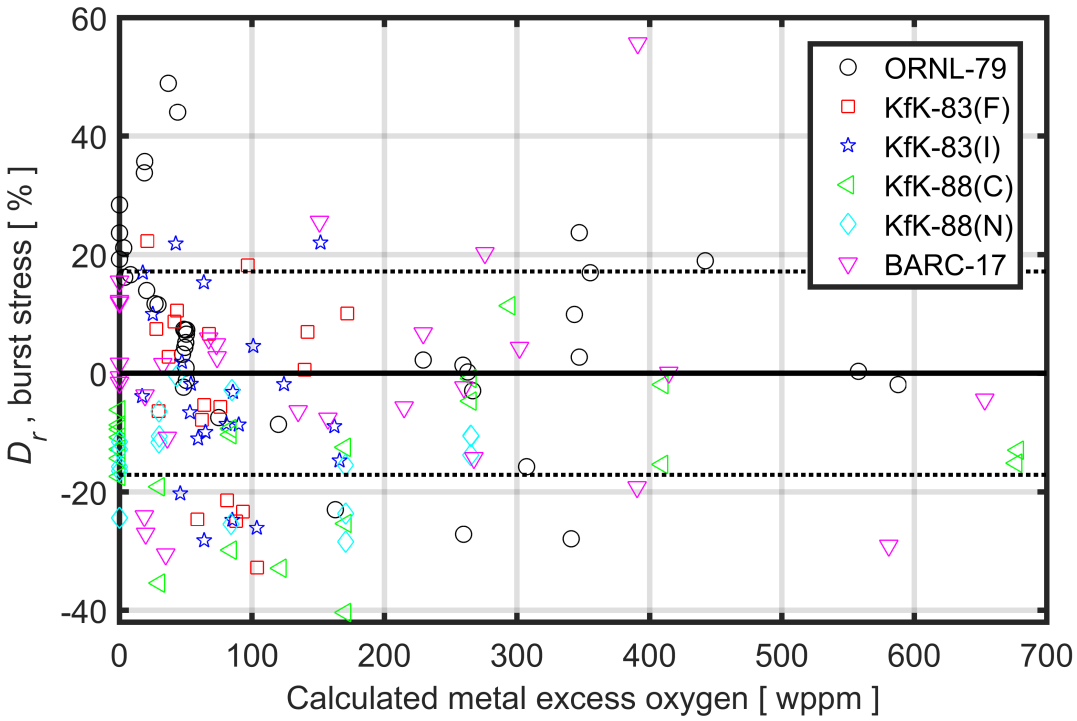

Figure B.12: Relative differences between calculated and measured burst hoop stress, plotted with regard to the calculated concentration of excess oxygen in the cladding metal (x_{Met}) at time of burst for each of the 151 test samples.

The Swedish Radiation Safety Authority has a comprehensive responsibility to ensure that society is safe from the effects of radiation. The Authority works from the effects of radiation. The Authority works to achieve radiation safety in a number of areas: nuclear power, medical care as well as commercial products and services. The Authority also works to achieve protection from natural radiation an to increase the level of ratiation safety internationally.

The Swedish Radiation Safety Authority works proactively and presentively to protect people and the environment from the harmful effects of radiation, now and in the future.
The Authority issues regulations and supervises compliance, while also supporting research, providing training and information, and issuing advice. Often, activities involving radiation require licences issued by the Authority. The Swedish Radiation Safety Authority maintains emergency preparedness around the clock with the aim of limiting the aftermath of radiation accidents and the unintentional spreading of radioactive substances. The Authority participates in international co-operation in order to promote radiation safety and finances projects aiming to raise the level of radiation safety in certain Eastern European countries.

The Authority reports to the Ministry of the Environment and has around 300 employees with competencies in the fields of engineering, natural and behavioral sciences, law, economics and communications. We have recieved quality, environmental and working environment certification.

Publikationer utgivna av Strålsäkerhetsmyndigheten kan laddas ned via stralsäkerhetsmyndigheten.se eller beställas genom att skicka e-post till registrator@ssm.se om du vill ha broschyren i alternativt format, som punktskrift eller daisy.

Strålsäkerhetsmyndigheten
Swedish Radiation Safety Authority
SE-171 16 Stockholm
Phone: 08-799 40 00
Web: ssm.se
E-mail: registrator@ssm.se

E-print AB, 2021